AFRL-RX-WP-TR-2010-4173

COLLABORATIVE RESEARCH AND DEVELOPMENT (CR&D)

Delivery Order 0059: Molecular Dynamics Modeling Support

Vikas Varshney

Universal Technology Corporation

MARCH 2008
Final Report

Approved for public release; distribution unlimited.

See additional restrictions described on inside pages

STINFO COPY

AIR FORCE RESEARCH LABORATORY
MATERIALS AND MANUFACTURING DIRECTORATE
WRIGHT-PATTERSON AIR FORCE BASE, OH 45433-7750
AIR FORCE MATERIEL COMMAND
UNITED STATES AIR FORCE

NOTICE AND SIGNATURE PAGE

Using Government drawings, specifications, or other data included in this document for any purpose other than Government procurement does not in any way obligate the U.S. Government. The fact that the Government formulated or supplied the drawings, specifications, or other data does not license the holder or any other person or corporation; or convey any rights or permission to manufacture, use, or sell any patented invention that may relate to them.

This report was cleared for public release by the USAF 88th Air Base Wing (88 ABW) Public Affairs Office (PAO) and is available to the general public, including foreign nationals. Copies may be obtained from the Defense Technical Information Center (DTIC) (http://www.dtic.mil).

AFRL-RX-WP-TR-2010-4173 HAS BEEN REVIEWED AND IS APPROVED FOR PUBLICATION IN ACCORDANCE WITH THE ASSIGNED DISTRIBUTION STATEMENT.

MARK GROFF
Program Manager
Business Operations Branch
Materials & Manufacturing Directorate

KENNETH A. FEESER
Branch Chief
Business Operation Branch
Materials & Manufacturing Directorate

This report is published in the interest of scientific and technical information exchange, and its publication does not constitute the Government's approval or disapproval of its ideas or findings.

*Disseminated copies will show "//Signature//" stamped or typed above the signature blocks.

REPORT DOCUMENTATION PAGE

Form Approved
OMB No. 0704-0188

The public reporting burden for this collection of information is estimated to average 1 hour per response, including the time for reviewing instructions, searching existing data sources, gathering and maintaining the data needed, and completing and reviewing the collection of information. Send comments regarding this burden estimate or any other aspect of this collection of information, including suggestions for reducing this burden, to Department of Defense, Washington Headquarters Services, Directorate for Information Operations and Reports (0704-0188), 1215 Jefferson Davis Highway, Suite 1204, Arlington, VA 22202-4302. Respondents should be aware that notwithstanding any other provision of law, no person shall be subject to any penalty for failing to comply with a collection of information if it does not display a currently valid OMB control number. **PLEASE DO NOT RETURN YOUR FORM TO THE ABOVE ADDRESS**.

1. REPORT DATE *(DD-MM-YY)*	2. REPORT TYPE	3. DATES COVERED *(From - To)*
March 2008	Final	10 August 2006 – 10 December 2007

4. TITLE AND SUBTITLE
COLLABORATIVE RESEARCH AND DEVELOPMENT (CR&D)
Delivery Order 0059: Molecular Dynamics Modeling Support

5a. CONTRACT NUMBER
F33615-03-D-5801-0059

5b. GRANT NUMBER

5c. PROGRAM ELEMENT NUMBER
62102F

6. AUTHOR(S)
Vikas Varshney

5d. PROJECT NUMBER
4349

5e. TASK NUMBER
L0

5f. WORK UNIT NUMBER
4349L0VT

7. PERFORMING ORGANIZATION NAME(S) AND ADDRESS(ES)
Universal Technology Corporation
1270 North Fairfield Road
Dayton, OH 45432-2600

8. PERFORMING ORGANIZATION REPORT NUMBER
S-531-0059

9. SPONSORING/MONITORING AGENCY NAME(S) AND ADDRESS(ES)
Air Force Research Laboratory
Materials and Manufacturing Directorate
Wright-Patterson Air Force Base, OH 45433-7750
Air Force Materiel Command
United States Air Force

10. SPONSORING/MONITORING AGENCY ACRONYM(S)
AFRL/RXOB

11. SPONSORING/MONITORING AGENCY REPORT NUMBER(S)
AFRL-RX-WP-TR-2010-4173

12. DISTRIBUTION/AVAILABILITY STATEMENT
Approved for public release; distribution unlimited.

13. SUPPLEMENTARY NOTES
PAO Case Number: 88ABW 2009-0426; Clearance Date: 01 Feb 2009.

14. ABSTRACT
This research in support of the Air Force Research Laboratory Materials and Manufacturing Directorate was conducted at Wright-Patterson AFB, Ohio from 10 August 2006 through 10 December 2007. This task performed molecular dynamics modeling research in support of thermosetting composites as well as nano-tailored composites for improving composite properties. The report focuses on the crosslinking procedure to build the crosslinked network or epoxy based composites. The crosslinked network is characterized with respect to various thermodynamic properties. The structure development during crosslinking stage is also focused. The thermal transport in crosslinked systems is discussed with the help of several analysis tools which are covered in the later part of the report along with the results regarding thermal interface resistance between crosslinked epoxy resin and CNT.

15. SUBJECT TERMS
nano-tailored composites, crosslinked systems

16. SECURITY CLASSIFICATION OF:			17. LIMITATION OF ABSTRACT:	18. NUMBER OF PAGES	19a. NAME OF RESPONSIBLE PERSON (Monitor)
a. REPORT	b. ABSTRACT	c. THIS PAGE			Mark Groff
Unclassified	Unclassified	Unclassified	SAR	58	19b. TELEPHONE NUMBER *(Include Area Code)* N/A

Standard Form 298 (Rev. 8-98)
Prescribed by ANSI Std. Z39-18

TABLE OF CONTENTS

Introduction	1
Heat Conduction	3
Molecular Dynamics Simulations	5
Theory: Equilibrium Molecular Dynamics Simulations	6
Theory: Non-Equilibrium Molecular Dynamics Simulations	8
Carbon Nanotube Simulations: Approach and results from equilibrium and non-equilibrium molecular dynamics simulations.	10
Epoxy networks systems of interest	13
Results: Curing Agent – W (DETDA) Thermal Conductivity	16
EPON Thermal Conductivity Results	17
Crosslinking Approach	20
Crosslinking Validations	27
Thermal Conductivity of Crosslinked Network from Non-Equilibrium Approach	33
Thermal Conductivity of Crosslinked Network from Equilibrium Approach	35
Power Spectrum Analysis	37
Pair Contribution Analysis	39
Thermal Diffusivity and Mean Free Path Analysis	42
Thermal Conductivity Simulations for CNT/Epoxy Interface	46

Introduction

The overall motivation and goal behind the current project was to understand the thermal transport in disordered networks in disordered networks at the molecular level using molecular dynamics simulations and connect it to microscopic level. The next likely step would be to take this understanding to Finite Element Modeling level so that this could be applied at macroscopic epoxy models to study their thermal behavior. This approach will result in making better thermally efficient epoxy composites with pre-determined thermal and mechanical characteristics.

Due to the inability of pursuing the simulations because of unavailability of computer resources, during the first three months of the project (Oct 2006-Dec 2006), research had been mostly focused on reviewing and understanding published literature regarding various thermal conductivity and multi-scale modeling techniques. "Simulations of epoxy resins/networks", "Simulations of thermal conductivity of ordered systems", "Multi-scale modeling of networks", "Thermal conductivity simulations in disordered systems".

From the literature search, we discovered that the subject of understanding thermal conductivity in disordered systems has rarely been touched from the perspective of molecular dynamics simulations. However, ordered systems such as "Carbon Nanotubes" have been investigated in terms of their thermal conductivity and good comparison with experimental results has been found.

Predominantly, there exist two procedures to calculate thermal conductivity, namely, a) Green-Kubo formalism and b) Fourier law methodology. These methods will be explained in detail later on in the report.

As mentioned above, the literature search was also focused on reviewing various approaches to scale the molecular models at coarse-grain level to study the systems at a microscopic level. Though, there are many different approaches taken by several authors, primarily two approaches have been used to coarse-grain the models successfully, namely a) Boltzmann inversion technique by Kremer et al. and b) Force-Matching algorithm by Gregory A. Voth. Although, the literature search was successfully performed for future simulations, the project mainly dealt with performing simulations atomistic level.

Since, the thermal transport on the ordered systems has been studied in literature in quite detail, we first studied the thermal properties of CNTs, in order to generate codes and familiarize with the field of thermal conductivity calculations from simulation perspective.

After that, we focus on thermal transport for disordered uncross-linked epoxy resin and curing agent-W (the constituents of epoxy networks). Once, the simulation and thermal analysis of these systems were convincingly done, we then focused on building a crosslinked network and study its thermal properties using equilibrium as well as non-equilibrium molecular dynamics simulation approach. Later on, simulations of CNT with epoxy resin interface were also performed to study how thermal interface resistance across the CNT/epoxy resin boundary.

Here, it is worth mentioning the order of the report.

First of all, the field of heat conduction is discussed briefly from fundamental and literature perspective. Then, molecular dynamics simulations are introduced as an alternative approach to experiments to tackle various molecular scale problems at nano- timescales. Thereafter, some theoretical background is discussed to calculate thermal conductivity using molecular dynamics simulations.

Once, the basic theory and fundamentals are presented, results from thermal conductivity simulations from CNTs are discussed briefly. Then, we would switch gear to disordered systems where we the heat transport is studied in un-crosslinked curing agent and un-crosslinked resin.

The report then focuses on the crosslinking procedure to build the crosslinked network or epoxy based composites. The crosslinked network is then characterized with respect to various thermodynamic properties. The structure development during crosslinking stage has also been focused. Thereafter, thermal transport in crosslinked systems has been discussed with the help of several analysis tools which will be discussed during the later part of the report.

Towards the end of the report, the results regarding thermal interface resistance has been discussed between crosslinked epoxy resin and CNT.

Heat Conduction

The thermal transport in solid materials is predominantly governed by the phenomenon of heat conduction. Heat conduction is a phenomenon, governed by Fourier law and states that the amount of heat transporting through a solid material per unit area in a unit time is directly proportional to the temperature gradient across the material[1]. The proportionality constant is broadly known as "thermal conductivity". The inverse of thermal conductivity is known as "thermal resistively". With the motivation of understanding the conductive or insulative properties, a great amount of research has been done to appreciate this phenomenon in significantly diverse class of materials which include metals, ceramics, alloys, composites materials, etc[1] in past few decades.

In ordered materials, the heat is transported using coherent vibrations, known as phonons[2]. The phonons are in general divided into two categories from the perspective of heat conduction, namely, acoustic and optical phonons. It is the acoustic phonons which give rise to heat transport in such systems. These vibrations are low frequency vibrations of much higher wavelength that that of IR-spectra. The main concept that differentiate the acoustic phonons which optical phonons is that fact that in former, the neighboring atoms moves in a same direction while in later, the neighboring atoms moves in opposite direction, like in stretching vibrations of C-H bonds.

On the other hand, the thermal transport in disordered/amorphous system is not discussed in terms of "phonon" as the vibrations get scattered quite easily before traveling any significant distance due to amorphous nature. Among such disordered materials, epoxy resin based thermo-sets and their composites presents a class of materials which possess excellent mechanical properties and hence, are often used in several structural components in aerospace and automobile industry[3]. However, it is well known from experimental results that these materials possess quite low thermal conductivity and are poor materials for thermal transport[4]. The issue of thermal transport through these epoxy networks becomes quite significant in situations where they are used as adhesive glues to join two thermally conductive materials, for example, in heat exchangers in aerospace applications, and hence presents a severe bottleneck for the thermal transport. It has also been shown experimentally that dispersing highly thermally conductive phases, such as CNTs and nano-particles, does not significantly enhance their thermal conduction properties, even above their percolation threshold limit[5]. The main reason behind this is known as Kaptiza resistance[6]. It is interfacial thermal resistance which happens wherever two materials subjected to thermal transport are allowed to be in contact. In such a case, the phonons from one material gets scattered at the interface, leading to un-efficient thermal transport across the other material. Such situations primarily lead to two possible solutions, a) to develop a thermally conductive pathway within the epoxy network or b) to tailor the intrinsic thermal properties of the adhesive network. Here, the latter alternative presents a clear motivation of understanding structure-property relationship of epoxy based networks, especially, in terms of possible thermal transport and will be studied as a part of this project from simulation perspective.

In this regard, molecular modeling provides a complimentary route to experiments to appreciate structure-property relationship. Not only modeling helps in analyzing the system at various length scales in a very cost effective manner without performing actual experiments, it also provides foundation for developing accurate theories and in designing better materials with tailored properties. Among various modeling techniques, molecular dynamics (MD) simulations (discussed later on)[7] present an opportunity to explore the system properties by assigning interaction parameters to its constituent elements (atoms) whose dynamics is governed by Newtonian equations of motion. To study epoxy networks, several groups have employed atomistic[8] as well as coarse-grained[9] molecular dynamics simulations to study their material properties. However, the literature has almost entirely been focused on studying the mechanical and structural properties of the systems, presumably due to their widely accepted role in building mechanically strong components with no reference to their thermal behavior.

In fact, quite a number of studies have been performed by several research groups in order to appreciate thermal properties at molecular level using MD simulations. Most of these studies have been performed on ordered systems such as Carbon Nanotubes[10], ionic salts[11], silicon[12], metals[13] etc. In such studies, thermal conductivity is often characterized in terms of propagation of well separated acoustic phonons through the system. However, the thermal behavior of amorphous or disordered systems such as epoxy composites has scarcely been touched from the perspective of atomistic simulations.

This provided us with the motivation to build a crosslinked network (of Epoxy Resins) and to undergo one of the first studies of thermal transport in disordered systems in detail.

Molecular Dynamics Simulations

Molecular dynamics simulation[7] is one of several simulation techniques which is quite powerful and gaining a lot of interest in exploring various phenomena occurring at pico- to nanosecond time scales. As these simulations consider atomic details, the effect of structure, molecular chemistry, etc. can be successfully studied on various physical properties. From the perspective of cross-linked networks, molecular dynamics simulations also possess inherent capability of addressing interface issues in composite materials. These interfaces are relatively sharp in nature and could only be treated as an approximate effective intermediate phase in continuum modeling.

The molecular dynamics simulations work in the principle of Newtonian equations of motion. At time scales of femto-seconds (the basic timestep of MD simulations), the forces are calculated for each atom based on pre-defined energetic potential. This potential include bonded (bond, angle, dihedral angle, improper angle) as well as non-bonded (van der Waals and electrostatic) interactions. Once, the forces are calculated and current velocities, the new co-ordinates of each atom is calculated based on basic Newton's equation of motion. There are several algorithms in literature to update the co-ordinates and velocities of the atoms as it evolves with time such as verlet algorithm, predictor-corrector method, etc.

In order to appreciate thermal transport from molecular simulation perspective, MD simulations provide two pathways, also known as equilibrium MD (EMD) and non-equilibrium MD (NEMD) simulations. These methods are based on Green-Kubo formalism[14] and Fourier law formalism[15], respectively. While EMD simulations are best suited for studying homogenous systems, NEMD simulations have an advantage when studying heterogeneous systems[16], although they can also be used to study homogenous systems. The theoretical background of these systems is discussed next.

Theory: Equilibrium Molecular Dynamics Simulations

Equilibrium molecular dynamics simulations are often used to calculate several transport properties using Green-Kubo (GK) approach[14]. This approach is based on fluctuation-dissipation theorem and relates the fluctuation properties of the thermodynamic system to its linear response properties. In other words, it provides a pathway to relate out of equilibrium properties (transport coefficients) with fluctuations in equilibrium properties. The transport coefficients are evaluated by integrating time autocorrelation functions of microscopic fluxes of equilibrium properties. Few of such examples include diffusion coefficient, thermal conductivity, electrical conductivity, viscosity, etc. In particular, the thermal conductivity, λ, using GK formalism is calculated by integrating time auto-correlation function of heat flux and is given by following equation.

$$\lambda = \frac{1}{k_B T^2 V} \int_0^\infty \langle \mathbf{J}(t) \bullet \mathbf{J}(0) \rangle dt$$

Here J(t) is the heat flux vector at time t. In addition, V and T represent the volume and temperature of the system, respectively, while k_B is the Boltzmann constant. In terms of molecular dynamics entities, J(t) is written as

$$\mathbf{J}(t) = \frac{d}{dt} \sum_{i=1}^{N} \mathbf{r}_i E_i \qquad \text{where} \qquad E_i = \frac{1}{2} m_i \mathbf{v}_i^2 + \frac{1}{2} \sum_{j \neq i}^{N} u(r_{ij})$$

Here, m_i and v_i represent mass and velocity of atom i. $u(r_{ij})$ is total potential energy of atom i whereas r_{ij} is the distance between atom i and j. In most cases, an analytic form of J(t) is used to evaluate J(t) which generally depend upon the form of interaction potential $u(r_{ij})$ employed in the simulations. In our case, we have used 12-6 Lennard Jones potential for non-bonded van der Waals interactions along with Ewald summation for electrostatic interactions. In such case, the final expression for microscopic heat current vector J(t) sum becomes

$$\mathbf{J}(t) = \frac{1}{2} \sum_{i=1}^{N} \left[m_i v_i^2 + \sum_{j \neq i}^{N} u(r_{ij}) \right] \mathbf{v}_i + \frac{1}{2} \sum_{i=1}^{N} \sum_{j \neq i}^{N} (\mathbf{r}_{ij} \mathbf{F}_{ij}^R) \bullet \mathbf{v}_i + \frac{1}{2} \sum_{i=1}^{N} \sum_{j=1}^{N} \mathbf{v}_i \bullet \overleftrightarrow{\mathbf{S}}_{ij}$$

In above equation F_{ij} represents the short range van der Waals force and real part of Ewald-Coulomb force. These forces are computed in real space. On the other hand, tensor S is evaluated in Fourier space. The elements of tensor S are written as

$$\mathbf{S}_{ij}^{\alpha\beta} = \frac{4\pi}{V} \sum_{\mathbf{k} \neq 0}^{\infty} B_{\alpha\beta} \frac{1}{k^2} e^{-k^2/4R_C^2} Z_i Z_j \cos(\mathbf{k} \bullet \mathbf{r}_{ij})$$

$$B_{\alpha\beta} = \delta_{\alpha\beta} - \frac{2|\mathbf{k}_\alpha||\mathbf{k}_\beta|}{|\mathbf{k}|^2} - \frac{|\mathbf{k}_\alpha||\mathbf{k}_\beta|}{2R_C^2}$$

where α and β denote the direction in reciprocal space, k represents reciprocal vector, R_C represents Ewald parameter while i and j are atom indices. In addition, Z_i denotes the charge on atom i. The detailed discussion for the inclusion of tensor S in heat current vector has already been discussed in literature previously[17]. Here it is sufficient to say that it is introduced to avoid divergences arising from the long range columbic interactions and takes care of forces due to long range Ewald interactions in Fourier space[18]. The justification to use relatively slower Ewald technique could be deduced from the fact that such a procedure to capture the long range interactions efficiently is well documented in literature[17,18] and the references there in.

Theory: Non-Equilibrium Molecular Dynamics Simulations

The Fourier law approach is based on the principle of heat conduction which states that under steady state conditions, amount of heat flow per unit area in unit time is directly proportional to the temperature gradient at the cross-section. This proportionality constant is better known as thermal conductivity and is shown below. This method for the calculation of thermal conductivity from molecular dynamics simulations is also known as direct method as it is quite analogous to experimental conditions.

$$\lambda = \frac{Q/A\Delta t}{dT/dz}$$

Here, Q is heat flow through the cross-section, A is the cross-sectional area, Δt is the time for which heat is flowing and dT/dz is the steady state temperature gradient. Once, the heat flow and temperature gradient is known from the simulation, the thermal conductivity is easily calculated using above equation. The calculation of Q and dT/dz from molecular dynamics simulations is discussed briefly below.

First of all, the system of interest is build as a long thin slab along one direction and is equilibrated at desired temperature and pressure. Next, the central part of the slab is heated to desired high temperature, T_{high} and is kept at that temperature while the end boundaries are cooled to desired low temperature T_{low}. In order to keep the regions at their specified temperatures, energy is continuously added and taken off from hot and cold region, respectively during the course of the simulation. In doing so, a temperature gradient is established across the slab. In order to calculate the temperature gradient, the slab is divided into pre-defined number of small slabs with equal thickness. Thereafter, the temperature of each slab is calculated as follows[19].

$$T_i = \frac{1}{3N_i k_B} \sum_{k=1}^{N_i} m_k v_k^2$$

where, N_i is number of atoms in i^{th} slab. Furthermore, calculated temperature for each slab T_i is averaged over the several pico-seconds to get a smooth temperature profile. To get the better statistics, the temperature profile is further blocked averaged over several blocks. At last, the temperature gradient is calculated by the slope of resulting temperature profile.

On the other hand, heat flux per unit area, $Q/A\Delta t$ is calculated as follows

$$\frac{Q}{A\Delta t} = \frac{1}{A\Delta t} \left\langle \frac{1}{2} \sum_{k=1}^{N_B} m_k (v_k^2 - v p_k^2) \right\rangle$$

where vp_k and v_k are the velocities of the atoms before and after rescaling to desired temperature, respectively. N_B is the number of atoms in the boundary layers. Once the temperature gradient and the heat flux are known, the thermal conductivity is calculated using above.

Carbon Nanotube Simulations: Approach and results from equilibrium and non-equilibrium molecular dynamics simulations.

First of all, thermal conductivity simulations were performed for (10,10) armchair carbon Nanotubes using EMD as well as NEMD simulations. The main reason to start off with carbon Nanotubes simulations initially was the fact that its thermal behavior has been studied to a significant extent in literature. The nanotubes were build using Amorphous cell builder in Material Studio. First of all, the CNTs were equilibrated using NVT and NPT simulations. Thereafter, equilibrium and non-equilibrium molecular dynamics simulations were run to calculate their thermal conductivity. For NEMD simulations, a temperature gradient was established across the Nanotube while keeping track of how much energy is being put in order to maintain that temperature gradient in a steady state. The temperature gradient is shown in Figure 2. On the other hand, for EMD simulations, thermal conductivity was calculated from the integration of heat flux autocorrelation function (shown in Figure 3) as discussed in previous section. The results for both types of simulations are listed as follows.

NEMD approach (~500W/mK) @ 300K
EMD approach (~1100W/mK) @ 300K

In the literature the values reported for the thermal conductivity are around ~500-3000 W/mK. The spread in literature values is attributed to method used, length of the carbon Nanotubes simulated as well as the interaction potential incorporated. The higher values are mostly obtained with longer Nanotubes with “Brenner” interaction potential which considers short as well as long range interactions. It is worth mentioning that our simulations were performed using “Tersoff” potential which only considers 3-body short range interactions. The use of Brenner potential for further simulations has been left for near future (due to its unavailability presently in LAMMPS molecular dynamics simulation package).

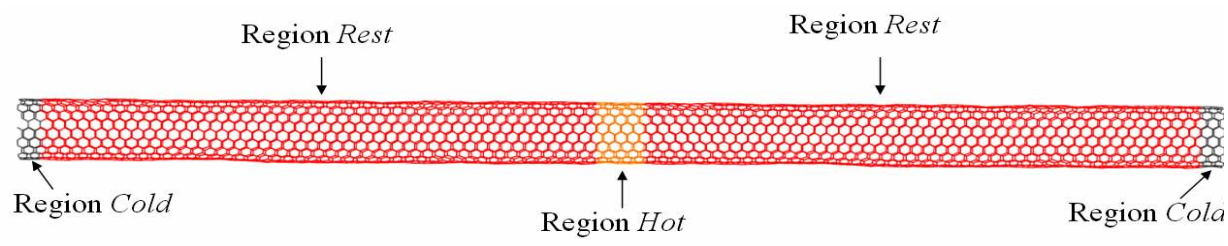

Figure 1: Schematic of CNT for NEMD simulations

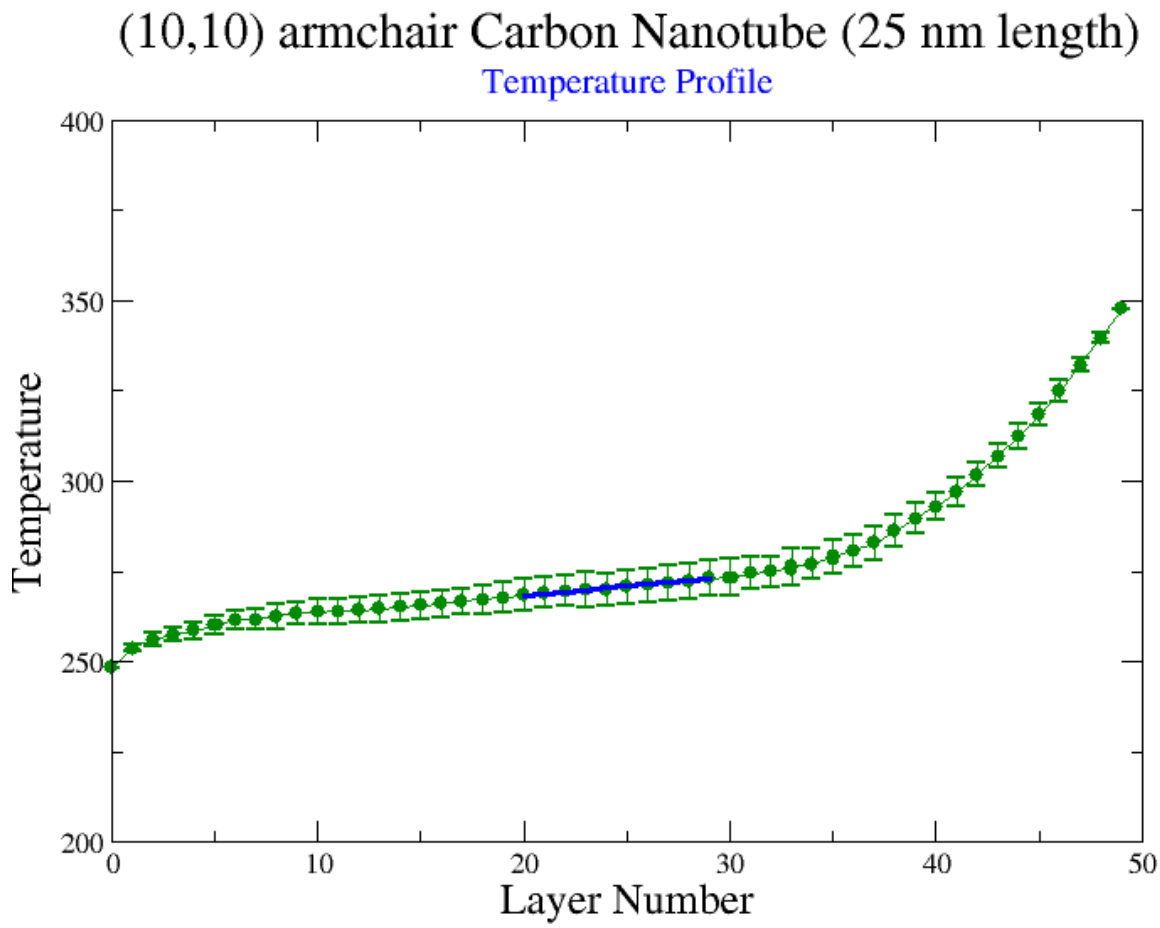

Figure 2: Temperature profile across Nanotube length.

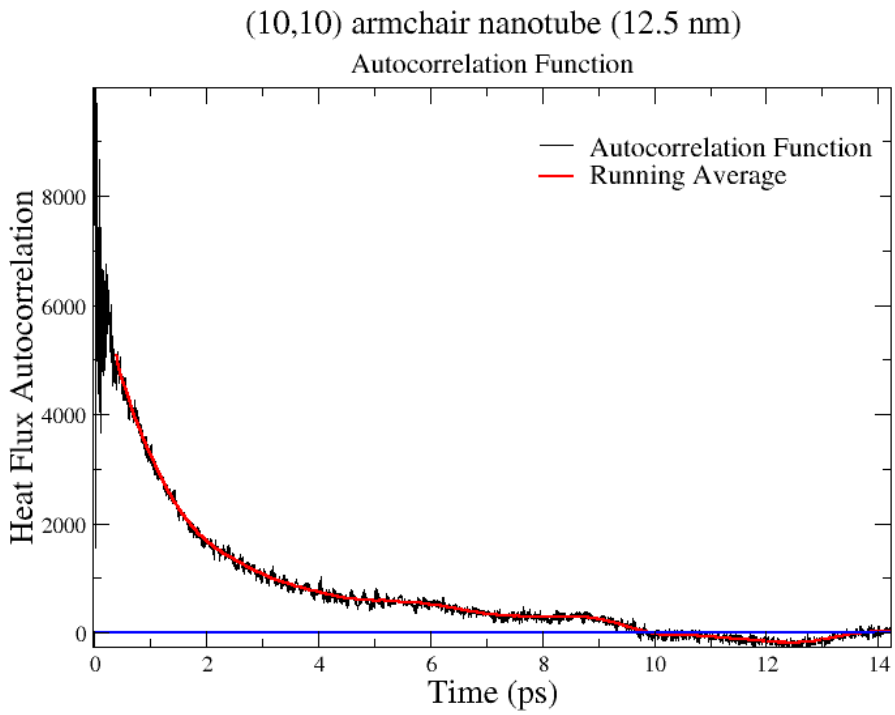

Figure 3: Decay of heat flux autocorrelation function for the carbon Nanotube.

Epoxy networks systems of interest

The system studied in current study consisted of epoxy resin, EPON-862, curing agent-W, also known as DETDA and their crosslinked network and are shown is shown in Figure 4 and 5 along with their crosslinking epoxy-amine reaction. For all simulations presented in this study, CVFF (Consistent Valance Force Field) potential was used for bonded as well as non-bonded interactions. In addition, for NEMD simulations, the long range electrostatic interactions were modeled using PPPM technique. However, since the heat flux equations use Ewald summation[20] to calculate electrostatic contributions, the relatively slower Ewald summation technique was employed for long-range electrostatic interactions for EMD simulations. All simulations were performed using open source LAMMPS (Large-scale Atomic/Molecular Massively Parallel Simulator) software provided by Sandia National Labs[21].

The initial configurations for both DETDA and EPON-862 were modeled using Material Studio®[22]. The system specifics after equilibration for each system along with crosslinked network are mentioned in Table 1. The crosslinking procedure in order to obtain a network is discussed later on. Here, we would like to mention that we were able to build a crosslinked network with relaxed structure and was characterized successfully in terms of thermodynamic, mechanical and structural properties. For current study, two crosslinked networks with ~87.5 % crosslinking was used for both equilibrium and non-equilibrium simulations.

Firstly, all three systems (un-crosslinked epoxy resin, curing agent and crosslinked network) were minimized using conjugate gradient method to remove possible overlaps between atoms. Thereafter, a constant volume (NVT) and constant pressure (NPT) simulations were run to equilibrate the temperature and density respectively. Once the initial equilibrated system was achieved, a series of equilibrium molecular dynamics and non-equilibrium molecular dynamics simulations were performed at room temperature.

For equilibrium molecular dynamics runs, after prior equilibration, a constant NVE simulation was performed for 100 pico-seconds to get the equilibrated structure in micro-canonical ensemble. Once, the system got equilibrated, further constant energy (NVE) simulations were performed on newly equilibrated system for data collection for 1.6 ns, where data were collected at 0.01 ps for the calculation of heat current vector and its subsequent analysis.

On the non-equilibrium simulations, the elongated slab was divided into 100 smaller slabs of equal thickness. In the central part of the system, 4 slabs were treated as hot region while the 2 slabs on each boundary were treated as cold region. The system was set to be periodic in all 3 dimensions. For current simulations, the hot region was kept at 350K while cold region was kept at 250 K. After the system is equilibrated from prior NPT simulations, the NEMD simulations in micro-canonical ensemble (NVE) were run for about 1ns in order to achieve steady state for heat flow. Once the steady-state was achieved, further simulations for 1.5 ns were run for the data collection at the interval of 0.1 ps for further analysis.

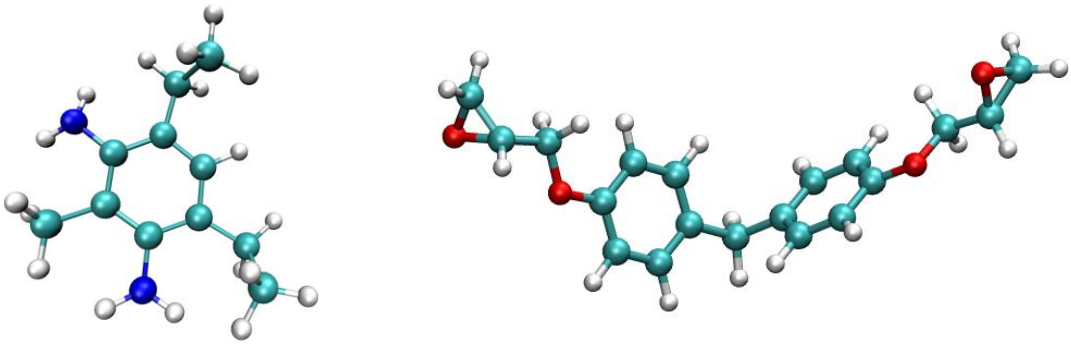

DETDA EPON-862

Cyan (CARBON); Red (OXYGEN); Blue (Nitrogen); White (HYDROGEN)

Figure 4: Starting systems DETDA and EPON-862. The depiction of colors is also listed above.

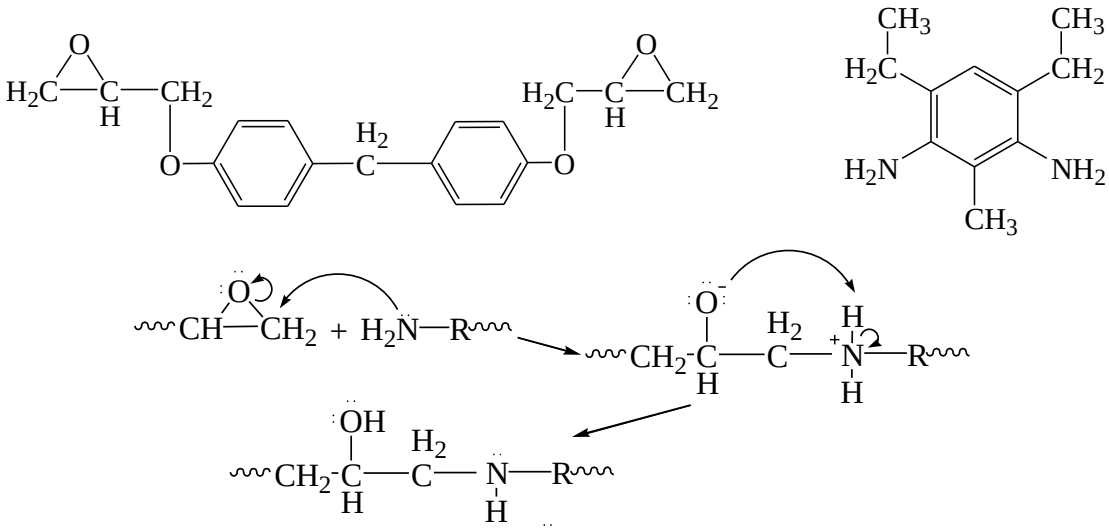

Figure 5: Crosslinking reaction.

Table 1: Specifications of systems studied

System Studied	Equilibrium MD		Non-Equilibrium MD	
	No. of Atoms	Dimensions (Å^3)	No. of Atoms	Dimensions (Å^3)
DETDA	9920	46.5 x 46.5 x 46.5	19840	23.3 x 23. x 373.3
EPON	4300	35.9 x 35.9 x 35.9	43000	35.9 x 35.9 x 359.9
Crosslinked System[1]	7538	42.56 x 42.56 x 42.56 (90.0)	15104	21.4 x 21.4 X 337.3 (90.0)
	14976	53.59 x 53.59 x 53.59 (87.5)		

[1] For the crosslinked system, stoichiometric ratio of EPON-862 and DETDA were used. For 2 cases mentioned in Table 1, (128, 64) and (256, 128) molecules were used for EPON-862 and DETDA, respectively. The numbers in ( ) signify crosslinking %. After the crosslinking procedure, the un-reacted entities were saturated with hydrogens.

Results: Curing Agent – W (DETDA) Thermal Conductivity

Equilibrium Molecular Dynamics

Figure 6a) shows the normalized heat flux autocorrelation function as obtained from equilibrium molecular dynamics simulations in X, Y and Z directions. It is observed from the figure that the autocorrelation function decays down to zero around ~6-8 ps. In addition, the figure also shows that all the autocorrelation functions in different directions are remarkably similar. This could lead to the fact that the system is indeed isotropic and homogenous.

Figure 6b) shows the final thermal conductivity in all 3 different directions as calculated by integrating the autocorrelation function, where the running average which serves as a guide to the eye is shown in red. The values of thermal conductivity in X, Y and Z directions were found to be 0.155 ±0.016, 0.184±0.017 and 0.153±0.009 W/mK respectively. The values in all 3 directions are quite similar in nature suggesting homogeneous nature of the system, providing the average thermal conductivity value of 0.16 W/mK.

Non-Equilibrium Molecular Dynamics

Figure 7 shows the normalized velocity distribution of the carbon atoms (C1, C2, and C3, as discussed in previous section), in different heating zones. In the figure, the velocity distribution in hot zone is shown as black curve while the grey curve shows the velocity distribution in the middle of thermostated zone. Both curves overlap each other quite nicely and are in close agreement with Maxwell-Boltzmann law for velocity distribution. This similarity, in addition to nice overlap suggests that there exists the local thermal equilibrium within the slab which confirms the use of non-equilibrium molecular dynamics simulations to calculate various thermal properties as discussed by Chatrenne et al.[23].

As mentioned before, to calculate the thermal conductivity from the NEMD simulations, one needs to make sure that the system does reach in a steady state (constant heat flux) before estimating temperature profile and heat flux. For our simulations, the steady state was reached after 1.2 ns as seen from the similar slope of both curves as shown in figure 8.

The steady state temperature profile for the DETDA system is shown in figure 9 where the temperature is plotted as the function of layer number. Each layer/slab was 3.73Å was estimated to be around in thickness. The temperature of each such layer was calculated as discussed in theoretical section, previously. In order to achieve better statistical results, the figure only shows averaged half system temperature profile from cold region to hot region. The figure also shows the calculated temperature gradient as fitted using least square fitting in the middle part of the temperature profile curve. The value of the temperature gradient is estimated as 1.96 K per layer (or 0.53 K/Å). After this evaluation, the thermal conductivity is estimated to be 0.2 W/mK. It is quite remarkable to see that the values from equilibrium molecular dynamics simulations and non-equilibrium molecular dynamics simulations are quite similar and also serves as an excellent guess, comparing with experimental results.

Here, it is worth mentioning that although, the current simulations were not focused on the effect of frequency of velocity update and the controlled (hot and cold region) slab thickness on the thermal conductivity, these variables should not make any significant difference in the values of

predicted thermal conductivity. The effect of such variables has been discussed in literature where the authors did not find any considerable change in the values of thermal conductivity as the function of slab thickness or frequency of velocity update.

EPON Thermal Conductivity Results

The epoxy resin thermal conductivity results will be discussed along with crosslinking network later in the report.

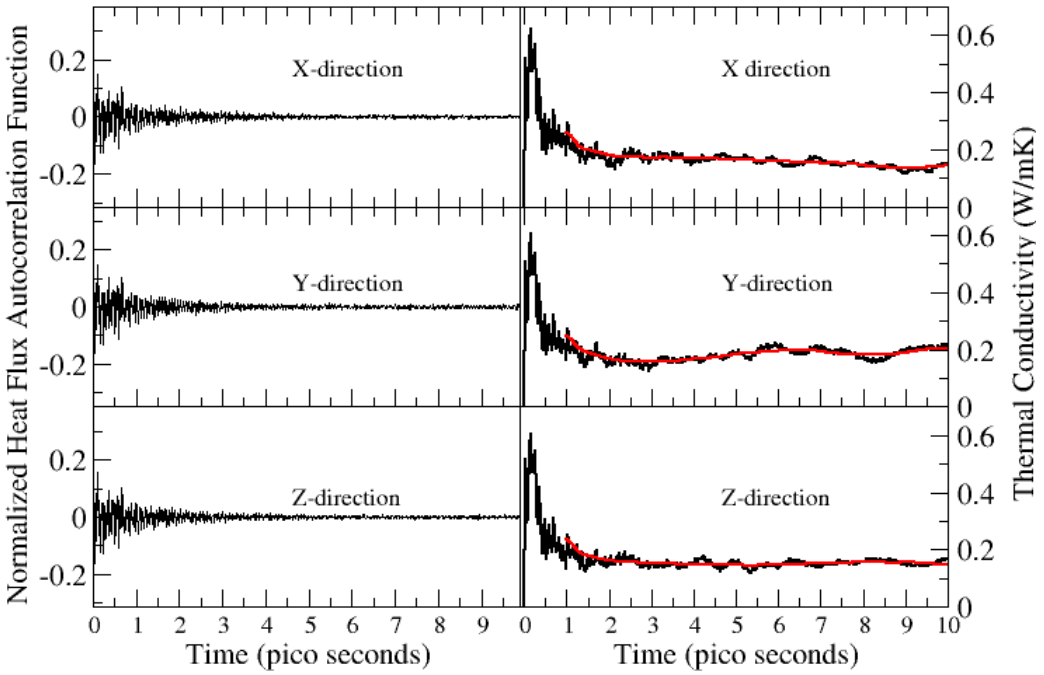

Figure 6: a) Normalized heat flux autocorrelation function as a function of time for 3 different directions. B) Calculated thermal conductivity for 3 different directions. The red

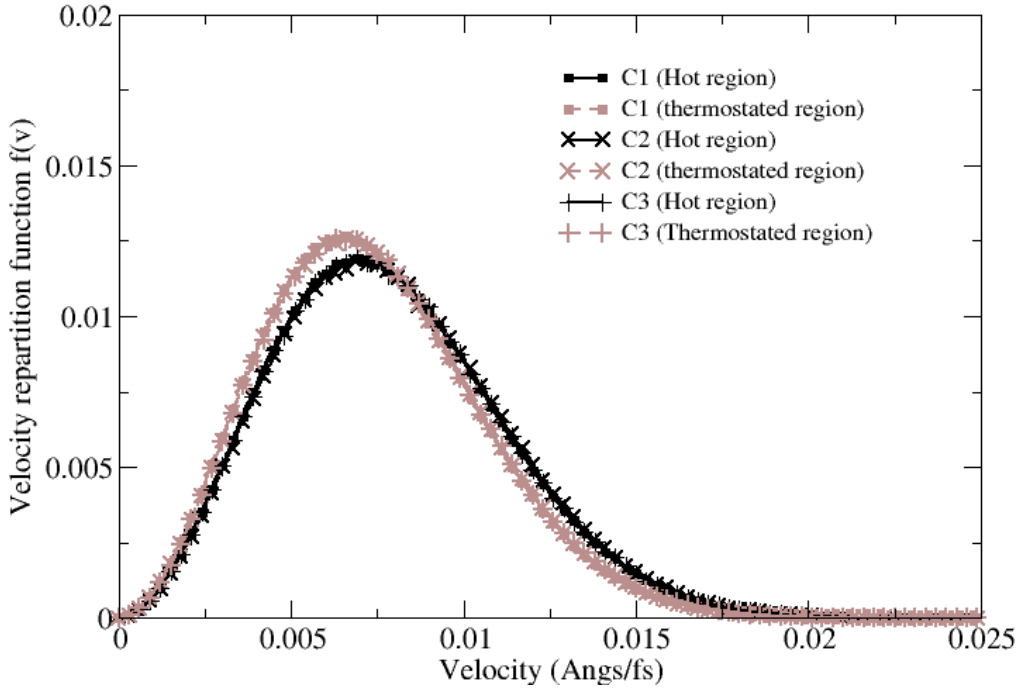

color represents the running average over the raw data.

Figure 7: Velocity distribution from non-equilibrium molecular dynamics simulations. Black: velocity distribution at the hot region. Brown: velocity distribution at the middle of the thermostated region.

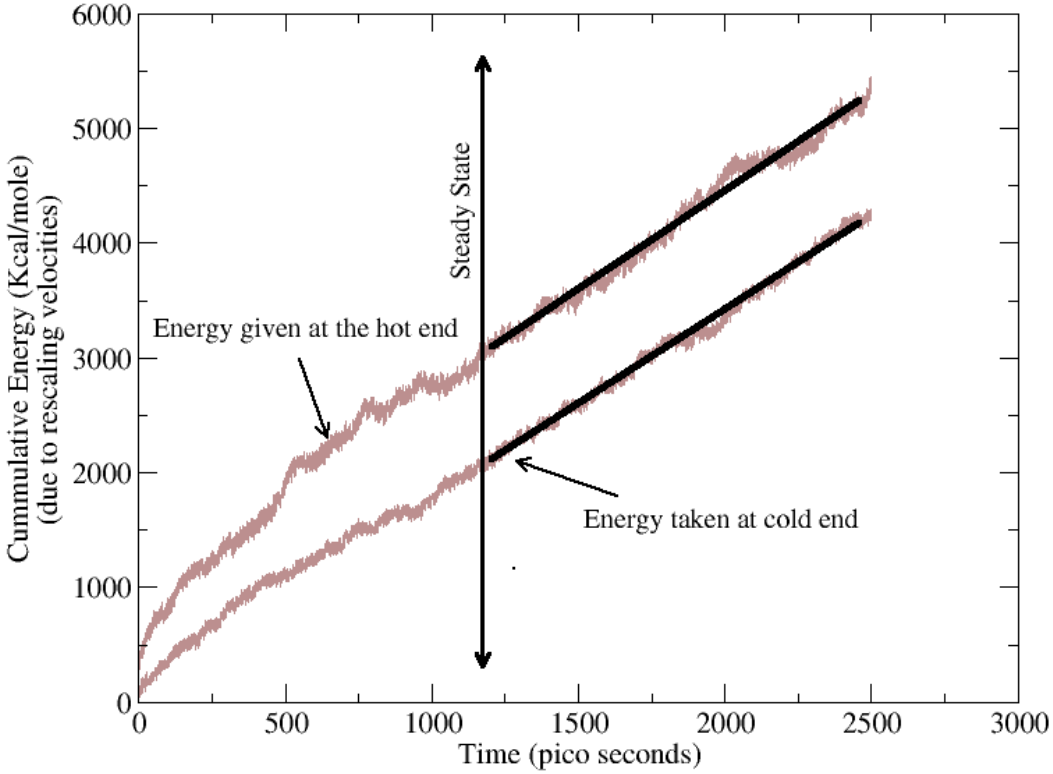

Figure 8: The heat flow across the DETDA simulation box along the length.

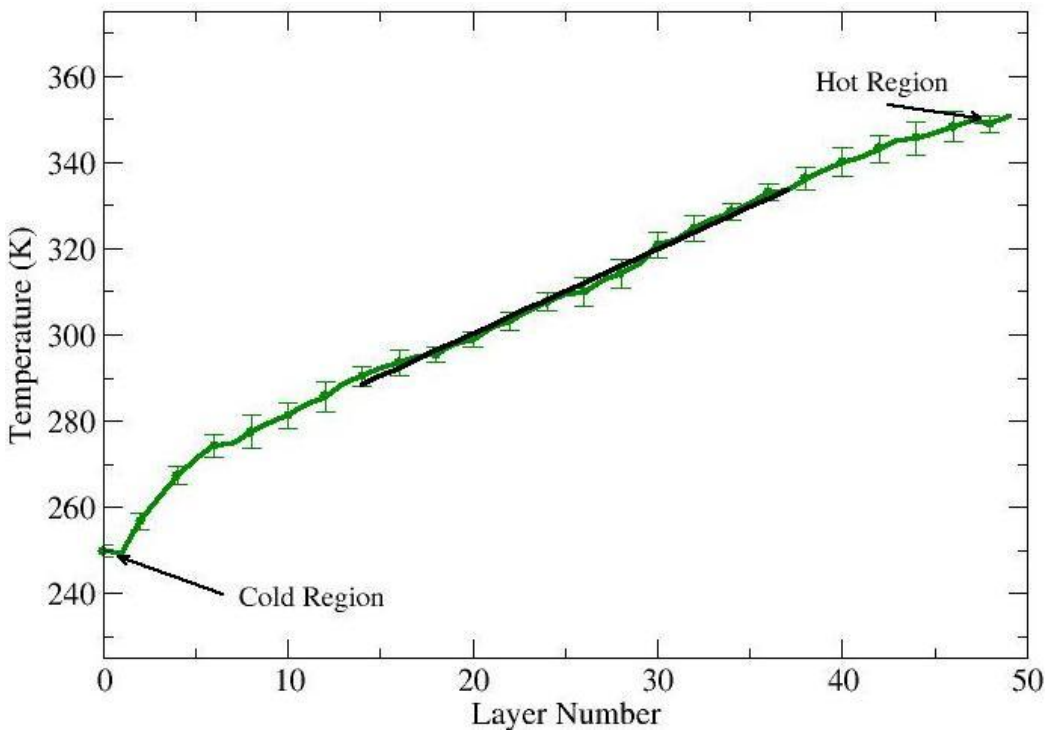

Figure 9: The averaged temperature profile (over both sides) as a function of layer number. Black solid line: fit to the points to determine temperature gradient.

Crosslinking Approach

Once, the thermal properties of the uncross-linked systems were calculated, next step was to crosslink the system. In this regard, 4 different crosslink strategies were taken into account which are discussed below. The crosslinking procedure was divided into 3 main steps, namely, activation, crosslinking and saturation.

Activation: In this step, all potential reactive sites are activated for both epoxy resin and curing agent as discussed by Xu[24]. This is done by first hydrating epoxy oxygen atoms at the ends and hence creating a reactive end methylene group. In case of curing agent, DETDA, both hydrogen atoms are removed to make it chemically active. In addition, the partial charges are also adjusted on these carbon and nitrogen atoms in respective molecules due to addition and removal of hydrogen atoms to keep the system neutral. The activation step is shown schematically in Figure 10.

Cross-linking Approaches:

Approach 1: This approach assumes equal reactivity of primary and second amine.

Approach 2: This approach assumes that primary amine has much higher reactivity than secondary amine. In this case, all the nitrogen atoms are reacted once before any secondary nitrogen reaction.

Approach 3: In this approach, a nitrogen is selected randomly and is fully reacted (twice) before any other nitrogen. This approach was employed to study dihedral energy buildup during the course of the cross-linking as discussed later.

Approach 4: It is the dynamic crosslinking approach. In this approach, all potential reactive pairs are reacted simultaneously within the cutoff in compliance with equal reactivity assumption.
The motivation for studying approaches 2 and 3 in addition to approaches 1 and 4 as studied by Xu[24] and Heine[9], respectively was to realize if they led to better equilibrated crosslinked structures with lower energies.

Crosslinking Algorithm: The crosslinking algorithm is shown in Figure 11a and 11b for cases 1-3 and case 4, respectively as a flow chart and is discussed below.

Step 1: In this step, initial cutoff distances as well as crosslinking limits (in terms of %) are defined for the crosslinking algorithm. For cases 1-3, upper bound cutoff distance (10 Å) was defined while for case 4, lower bound cutoff distance (4 Å) was defined. Although the crosslinking limit was set to be 100% originally, the simulations could be stopped at any time.

Step 2: In this step, system is equilibrated using NPT simulations for 40 pico seconds (10 ps of equilibration at elevated temperature, 600K; 25 ps of annealing to 300K followed by 5ps of equilibration at 300K). For the determination of equilibration time, first of all, RMSD (root mean square distance) of reactive carbon and nitrogen atoms was estimated. In 40 pico-seconds, RMSD of nitrogen and carbon atoms were calculated to be ~4.6 and 4.2 Å, respectively. The

estimation of equilibration time using this approach make sure enough random movement of reactive species before each crosslinking reaction and ensures that the reaction is indeed happening in a pseudo-equilibrium fashion.

Step 3: In this step, all potential un-crosslinked reactive pairs are identified. In addition, all pairs that pertain to possible catenation in the network are removed from the possible reaction. For cases 1-3, the minimum distance pair is then selected and a bond is formed if its distance is less than the cutoff distance. On the other hand, for case 4, all bonds within the cutoff distance are created.

Step 4a: If crosslinking does occur, the topological information is updated by introducing new bonds, angles, dihedral angles and improper angles into the system. Thereafter, the topology is relaxed using a multi-step relaxation procedure. This procedure essentially resists the abrupt change in the co-ordinates of atoms in the vicinity of newly formed bond and ensures the slow relaxation of atoms comprising of newly formed topology. In this procedure, the force constant of the newly formed bond is gradually increased from zero to its equilibrium value in a series of steps. Similarly, the equilibrium bond length of the new bond is gradually decreased from original distance to its actual equilibrium value. The system is minimized at each step with effective bond parameters. For our cases, we used five such steps as shown in Table 2.

Step 4b: If crosslink does not occur, the system is further equilibrated according to step 2. However, for case 4, the cutoff distance is increased by 0.25 Å for the next iteration.

Step 5: After the minimization, if crosslinking limit is not reached, the algorithm jumps to step 2 where the equilibration of the new structure is performed; else the simulations are stopped.

Saturation: Once the crosslinking algorithm finishes, the remaining active sites on both un-reacted amine nitrogen atoms and epoxy carbon atoms are saturated with hydrogen. Here charges on these complementary atoms are also adjusted to keep the system neutral. Although, it is a subtle point, but it is worth noticing that once a crosslink is created between amine nitrogen and epoxy carbon, the charge distribution around these atoms is going to be different than if the crosslink was not been formed. In order to rectify this problem, charges were evaluated on a model molecule, as shown in Figure 12 which has the similar topology as around newly formed crosslinks. Then, the original charge distribution around the new crosslinks was replaced by charge distribution shown in Figure 12, in the shaded region keeping the system neutral.

In order to achieve a relaxed crosslink network, the system is further equilibrated at zero pressure using constant pressure simulations by first heating at 600 K for 100 pico seconds followed by annealing to 300K in 6 nano seconds.

Although, the above methodology has been discussed for system sizes of (16, 8), we also performed crosslinking simulations for relatively larger (128, 64) systems in 2 different geometries (cube and slab) using dynamic crosslinking approach as discussed above, the main motivation being the evaluation of thermal properties as discussed later. The use of this dynamic crosslinking approach over other approaches should become more transparent during the discussion concerning comparisons of different approaches used to crosslink (16, 8) systems.

While, the results from (16, 8) simulations are used to compare different approaches in terms of buildup of intra- and inter-molecular energies as a function of crosslinking, the results from (128, 64) simulations are used to analyze different thermal, thermodynamic and structural properties. It will also be shown that some quantities such as volume shrinkage during crosslinking are not convincing extracted from (16, 8) simulations, however, they come out quite nicely with relatively large (128, 64) systems.

Below, results from various cross-linking approaches are discussed for smaller (16, 8) systems. In this regard, various intra- and inter-molecular energies along with their computational times have been listed in Table 3 for un-crosslinked vs. crosslinked system using different approaches.

The important points from the table are as follows

- All energies except columbic energy are increased with respect to un-crosslinked system.

- The rise in bond, angle and dihedral energies could be attributed to newly formed topology.

- The increase in van der Waals energy is due to the increase in number of 1-4 interactions. The CVFF force field treats 1-4 interactions as non-bonded interactions.

- Dynamic cross-linking approach (approach 4) lead to better equilibrated crosslinked structure in terms of various intra- and inter-molecular energies. Here almost all energies are at least among all studied approaches.

- Dynamic crosslinking approach also has an advantage with respect to computational time over other approaches. In further support of dynamic crosslinking approach, we would like to point out that for the crosslinking of larger (128, 64) system with 256 possible crosslinks, ~95% crosslinking was achieved in only 75 iterations. Hence, it shows a significant reduction in computational time for crosslinking ($1/3^{rd}$) with respect to other 3 approaches which would take more than 250 iterations on the whole for same amount of crosslinking.

One of the interesting things is to observe the proximity of reactive sites during the crosslinking stage using various approaches. One of such results is shown in Figure 13 where the initial distance at which bond is formed is shown as the function of crosslinking % with dynamic crosslinking procedure for (128, 64) cube system. As seen from the figure, about 80% and 90% of the crosslinking has been successfully achieved within the cutoff distance of 4 Å and 5.5 Å, respectively. When compared to experimental crosslinking where 60-70% crosslinked is reached generally, the figure clearly shows that using the dynamic crosslinking approach as discussed before, a well-relaxed crosslinked network can be attained successfully without imposing any crosslinking strain within significantly less time as compared to other approaches. The final crosslinked structure is shown in figure 14.

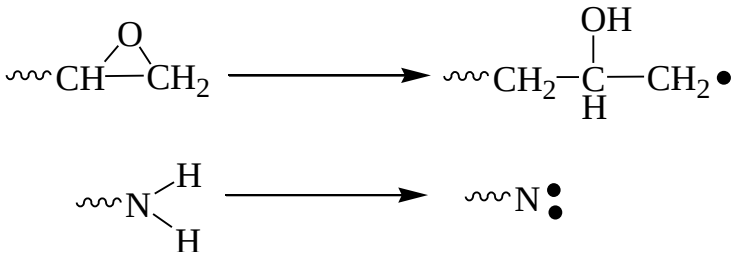

Figure 10. Activation of epoxy and amine ends for the cross-linking reaction

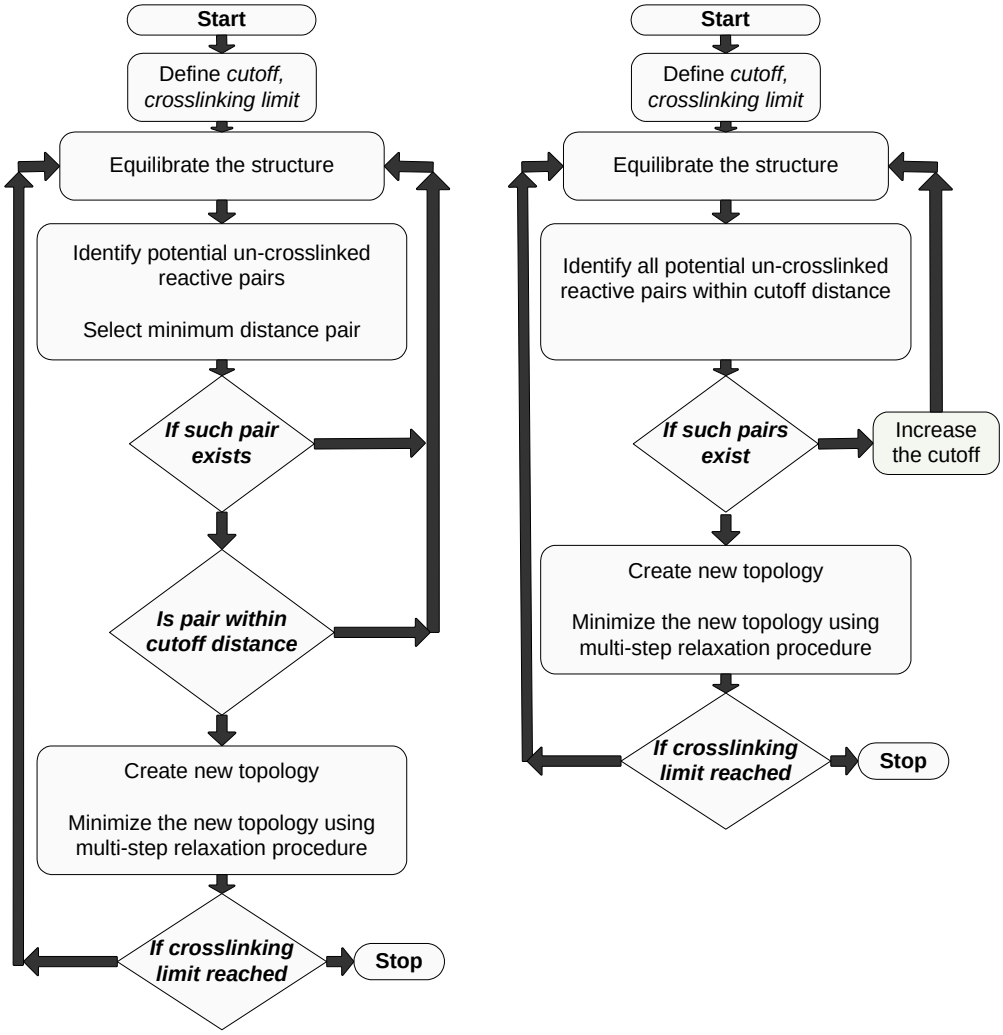

A **B**

Figure 11. Crosslinking algorithm. A) for approach 1-3 and B) for approach 4.

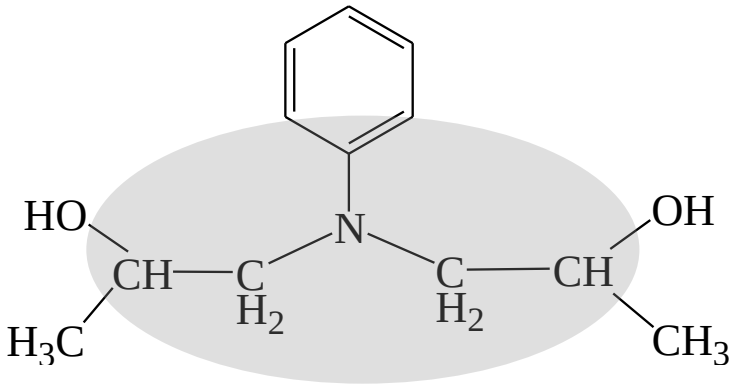

Figure 12: The shaded section of the molecule represents the cross-linking surroundings in which charges were redistributed.

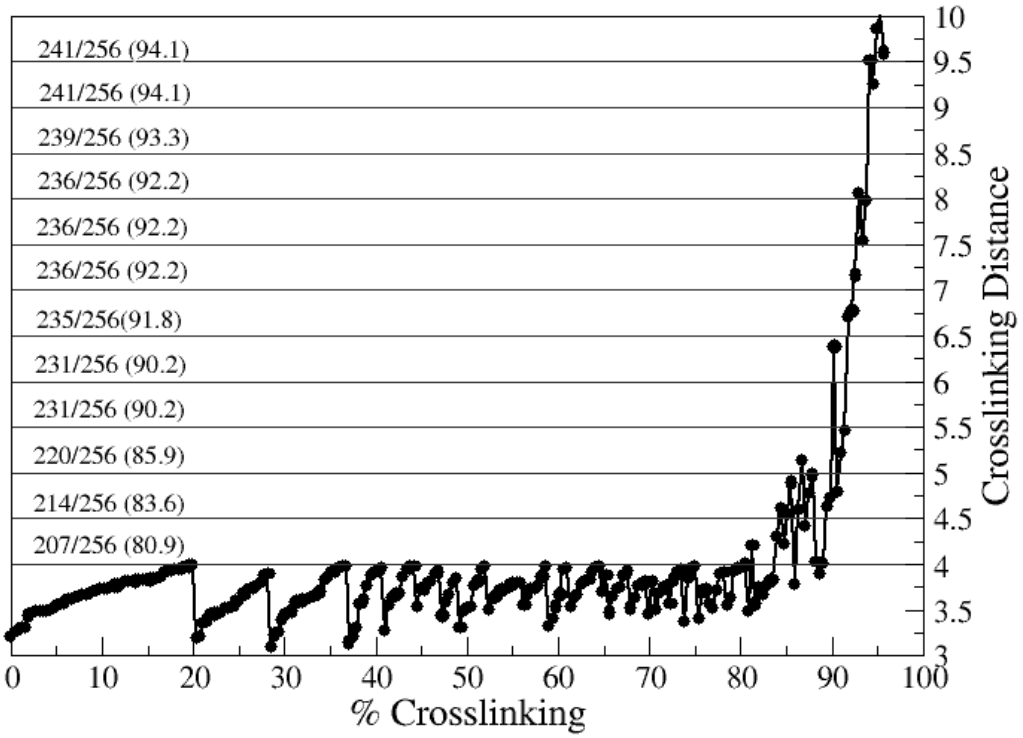

Figure 13: Plot of initial bond formation distance as a function of crosslinking.

Table 2: Multi-step relaxation procedure

No of steps	Effective Force constant[2]	Effective equilibrium bond length[3]
Step 1	$k_0/5$	$r_0 + 4\times(r - r_0)/5$
Step 2	$2\times k_0/5$	$r_0 + 3\times(r - r_0)/5$
Step 3	$3\times k_0/5$	$r_0 + 2\times(r - r_0)/5$
Step 4	$4\times k_0/5$	$r_0 + 1\times(r - r_0)/5$
Step 5	k_0	r_0

Table3: Comparison of various crosslinking approaches

Quantities[4]	Un-crosslinked System	Crosslinked Systems (30/32 cross-links)			
		Apprch. 1	Apprch. 2	Apprch. 3	Apprch. 4
Bond Energy (per unit)	419 (0.44)	471 (0.48)	473 (0.48)	472 (0.48)	468 (0.48)
Angle Energy (per unit)	99 (0.06)	165 (0.09)	172 (0.1)	168 (0.1)	164 (0.09)
Dihedral Energy (per unit)	129 (0.06)	440 (0.18)	441 (0.18)	418 (0.17)	423 (0.17)
van der Waals Energy	580	774	758	774	754
Columbic Energy	-349	-355	-335	-341	-350
Total Energy	231	419	423	433	404
Computational Time[5] (iterations)	N/A	32	32	31	23

[2] k_0 defines equilibrium force constant

[3] r_0 defines equilibrium bond length

[4] Energy units are in Kcal/mol. per unit quantities for respective energies are shown in ().

[5] The computational time is given in terms of number of iterations since every iteration has same equilibration time (per iteration) irrespective of the approach.

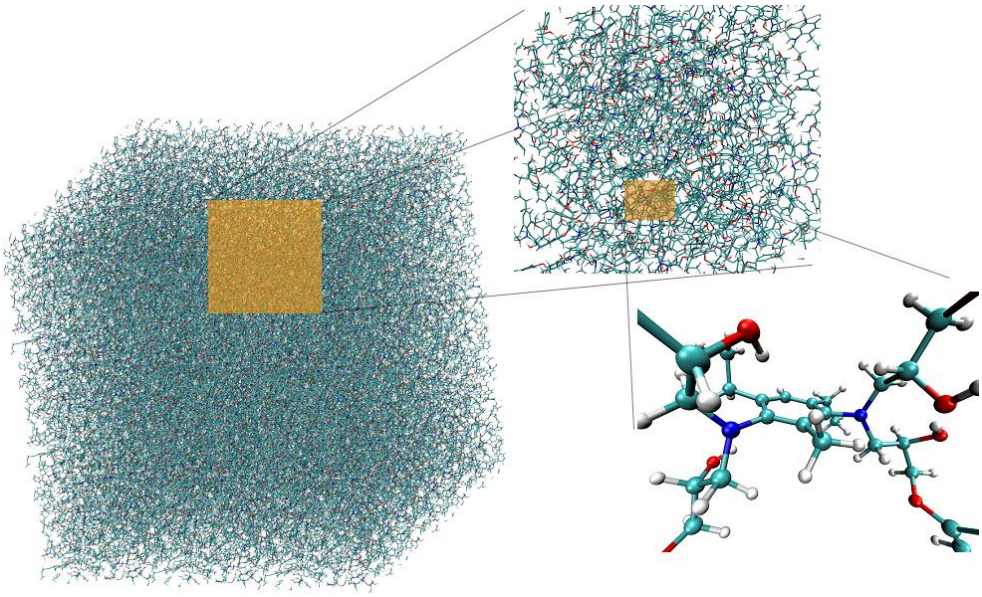

Figure 14: The crosslinked network.

Crosslinking Validations

For the validation, various material properties were analyzed for (128, 64) system. Here, the results will be presented from cube geometry. However, it should be mentioned that similar results were found for slab geometry also.

One of the properties which is directly evident during the process of network formation in experiments is the volume shrinkage. It has been reported in literature that for epoxy based networks, the change in volume accounts for ~7-8% (shrinkage) for densely crosslinked systems. In order to observe this shrinkage, the instantaneous volume of the system during the crosslinking simulations was tracked continuously. In this regard, the resulted equilibrated volume as curing progresses is shown in Figure 15. It is quite interesting to note that for the crosslinking of highly dense system (~90% crosslinking), the volume shrinkage of 7% was observed in our simulations which is in good agreement in experimental findings, given the complexity of curing process. It is also important to notice here that such a volume shrinkage was not convincingly observed in case of smaller (16, 8) systems due to significant statistical variations as shown in inset of figure 15.

In order to study the temperature dependence of various thermodynamic quantities, an annealing simulation was performed where the crosslinked system was slowly cooled down at the rate of 10K/200ps from 500K to 200K under atmospheric pressure which was controlled by Nose-Hoover thermostat and barostat. In this regard, the change of density of the cured network as a function of temperature is plotted in Figure 16. The density at room temperature is found to be 1.12 which is in good agreement with experiments[25]. Apart from the expected negative slope of density vs. temperature, a kink is observed in figure 16, where the change of slope occurs. The kink is usually identified as the glass transition temperature (T_g) which in our case occurs around 105 ^{o}C. The glass transition temperature is a second order transition and its value is often governed by cooling rate as well as method of measurement. In case of our systems, the predicted T_g from our simulations are in fair agreement with experimental[25] as well as simulation results on similar systems, providing rationalization for studied annealing rate.

Coefficient of thermal expansion is another thermodynamic property which is of great importance in composite materials as they are used at various temperatures in practical applications. The coefficient of volume thermal expansion (CVTE), α, is defined as

$$\alpha = \frac{1}{V}\left(\frac{\partial V}{\partial T}\right)_P$$

where, V, T and P are the volume, temperature and pressure of the system respectively. For isotropic materials, the coefficient of linear thermal expansion (CLTE), β, is related to α as

$$\beta = \alpha/3$$

In this regard, the fractional change in volume (dV/V) vs. temperature is plotted in Figure 17. As expected, a kink is observed around 105 ^{o}C, suggestive of glass transition temperature.

Additionally, the slope from the figure 17 can be identified as CVTE, α. From above equations, the calculated values of CLTE were found to be 40 ppm/^{o}C and 90 below and above the glass transition temperature. Given the fact, that the annealing was done on highly crosslinked network (~90% crosslinked), one could say that the predicted values are in fair agreement with experimental findings.

In addition to thermodynamic properties, it is also important to appreciate different kinetic processes during the course of network formation. The processes are governed by reaction rates of various reactions and are often analyzed in terms of molecular weight build up, its distribution, cycle ranks, gel point, etc. using experimental techniques such as chromatography, etc. These processes eventually define the molecular structure of the crosslinked network. Here, we present few of such results in order to support our cross-linking approach from reaction kinetics perspective.

In this regard, weight average molecular weight, M_w is shown as a function of cure conversion in Figure 18. The figure shows that most of the rise in the molecular weight happens towards higher cure conversion (~0.65-0.75). This trend of molecular weight build-up is in accordance with the principle of step-growth polymerization, the same approach which is used to cure epoxy resins experimentally. From theoretical perspective, the figure also shows the build of molecular weight of largest group within the system, the inception of secondary cycles and their trend, along with theoretical gel point (0.574) as predicted by kinetic theory for bi-functional epoxy resins and tetra-functional cross-linkers. A secondary cycle is defined as an intra-molecular reaction happening within a group. The inception of the secondary cycles has also been treated as a gel point in literature. From the figure, it is quite clear that in our simulations, the inception of secondary cycles occur around 0.57 providing nice agreement between simulation results and theoretical predictions. The gel point can also be estimated from the inflection point of largest group molecular weight build up. Although it is quite difficult to identify the inflection point with great accuracy from figure 18, one can safely say that it seems to be occurring between 0.6 and 0.65, providing a good estimation of gel point. Here, we would also like to point that that towards higher cure conversion (>0.8), most of the reactions happening are intra-molecular reactions. This is supported by the fact that in this region, a linear increase in number of secondary cycles are observed as a function of cure conversion along with negligible build up of molecular weight.

It is known from the literature that near gel point, the probability of reaction between largest and second largest group is maximum. The reasons being, a) it gives rise to sharp increase in molecular weight of largest group, i.e., inflection point and b) after this reaction, most of the reactions are going to occur within this largest group and hence it also corroborates with the concept of inception of secondary cycles. In this regard, Chiu and co-workers[26] performed Monte Carlo simulations on curing of epoxides with amines and estimated the gel point using weight averaged reduced molecular weight (RMW) approach. RMW is defined as the average molecular weight of all reacting groups except the largest one. One can easily foresee that the RMW first increases with cure conversion and then decreases. Here, the maximum in RMW is also characterized as a gel point. In order to compare our approach with Chiu et al., we have also estimated the gel point using RMW approach. The results are presented in Figure 19 where molecular weight of largest, second largest and weight averaged reduced molecular weight is

plotted as a function of cure conversion. It is clear from the figure that maximum in second largest as well as RMW occur within close proximity of the theoretical get point which provided us with confidence in our cross-linking approach. Here, it is worth mentioning that both peaks in Figure 19 are quite broad due to limitations of system size (only 256 possible cross-links). However, we predict that the broadness of these peaks should decay down with the size of the system.

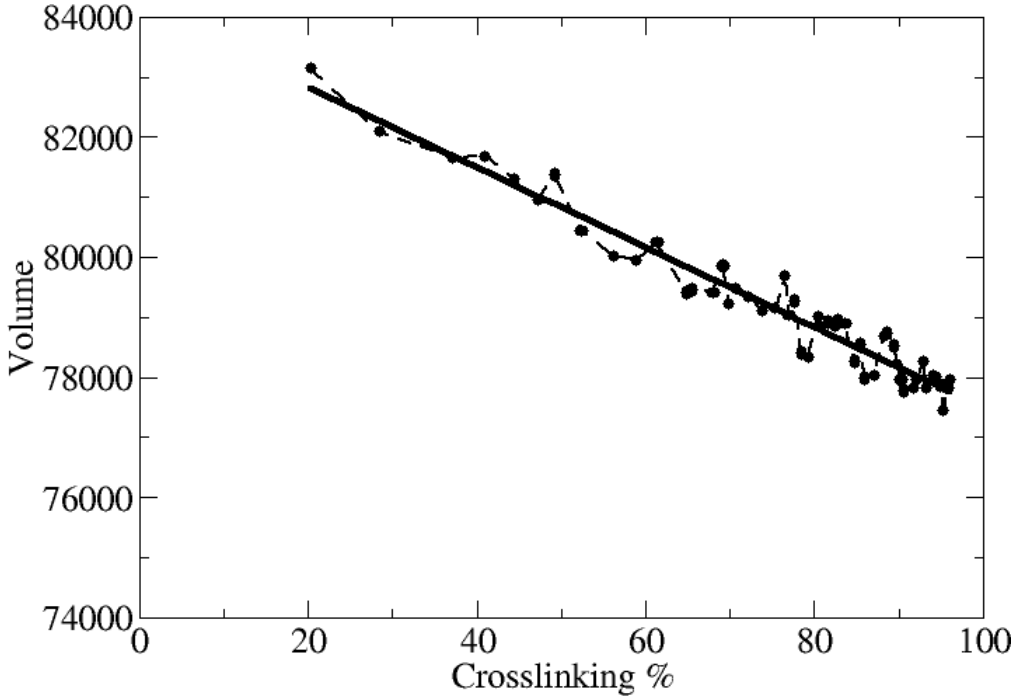

Figure 15: Plot of volume shrinkage as a function of cross-linking %.

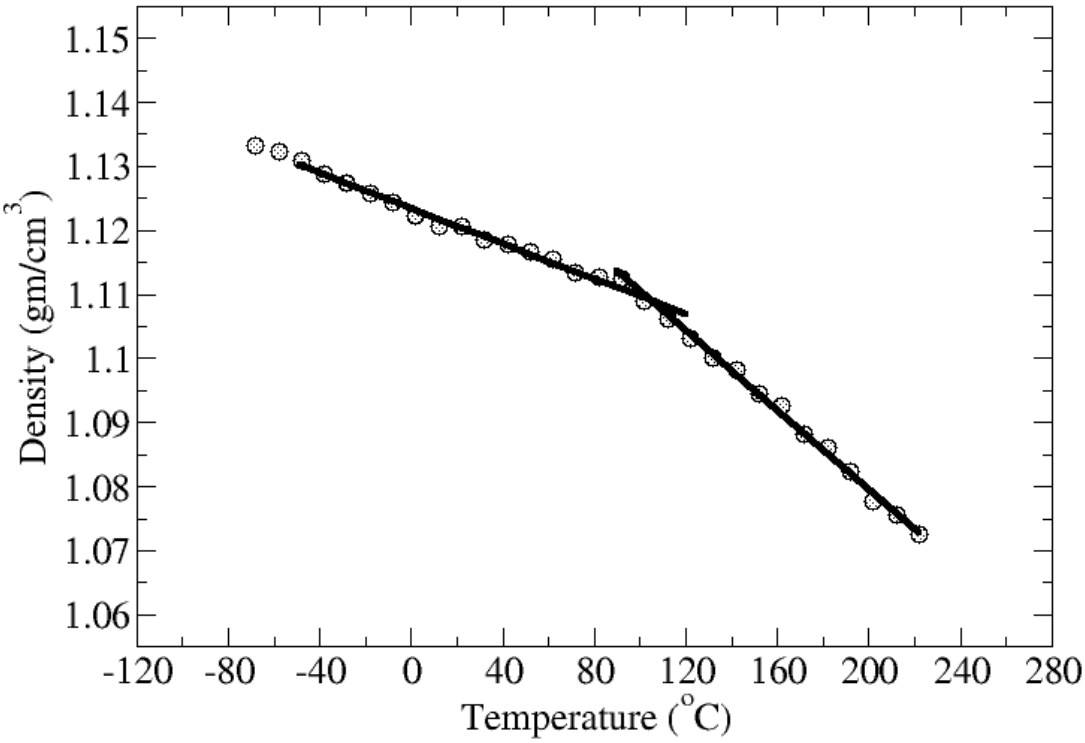

Figure 16: Plot of density variation as a function of temperature

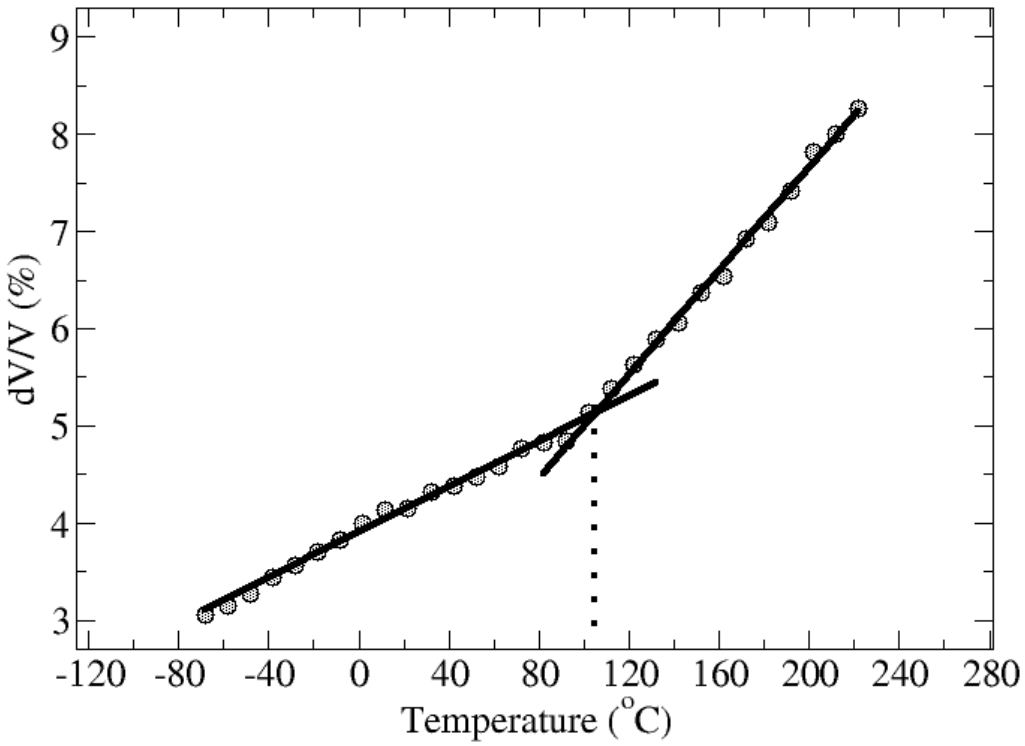

Figure 17: Plot of fractional volume change as a function of temperature

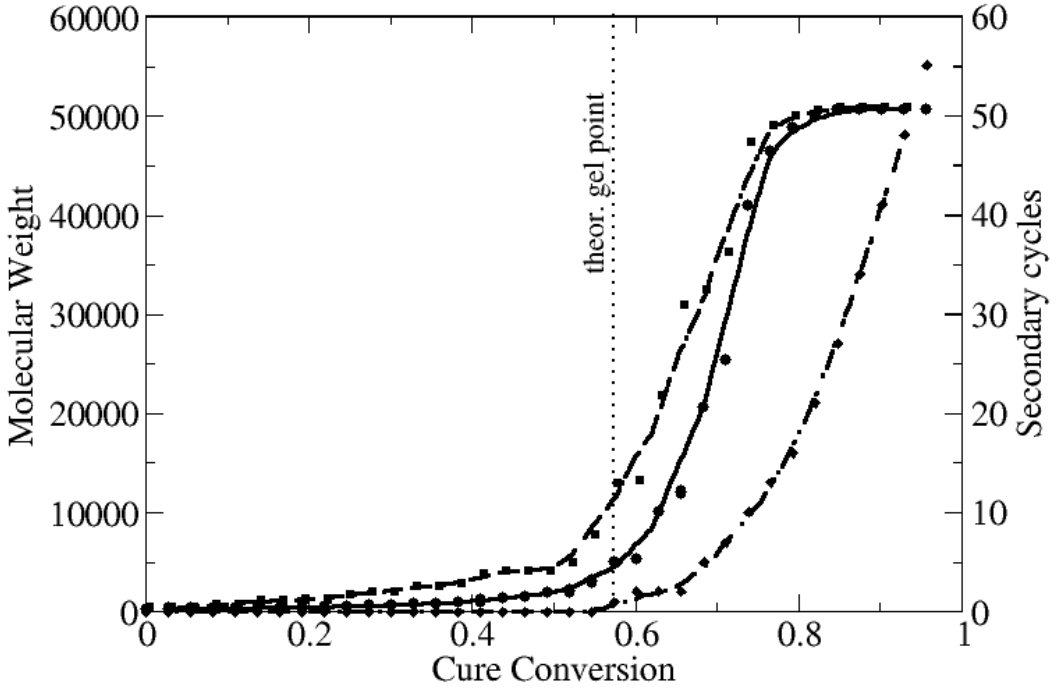

Figure 18: Plot weight average molecular weight (circles), largest molecular weight (squares) and secondary cycles (diamonds) as a function of cure conversion. The dashed lines are guide to the eyes.

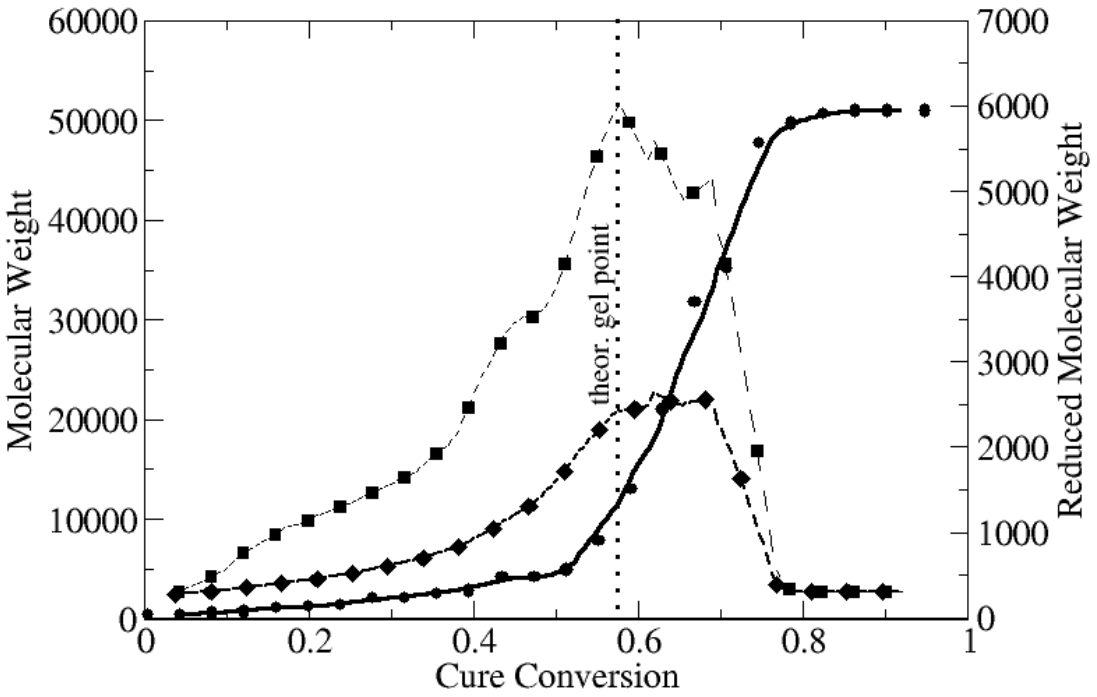

Figure 19: Plot of largest molecular weight (circles), second-largest molecular weight (squares) and weight averaged reduced molecular weight (diamonds) as a function of cure conversion. The dashed lines are guide to the eye.

Thermal Conductivity of Crosslinked Network from Non-Equilibrium Approach

The thermal conductivity calculations from non-equilibrium MD simulations were done on the basis of Fourier Law approach as discussed in the previous section. It has been suggested in literature[23] that for NEMD simulations to be justifiable, there should exist a local thermal equilibrium within the slab. For our simulations, this was confirmed by verifying the fact that the velocity distribution indeed followed the Maxwell-Boltzmann curve for thermostated as well as un-thermostated regions as discussed previously. After that, the heat flux and temperature gradient for calculated for all studied systems, namely, EPON-86, DETDA and crosslinked network. In this regard, Figure 20 shows the input (energy put in hot region) and output (energy taken off from cold region) energies as the function of simulation time in a cumulative manner for all 3 systems. From the figure, it should be safe to assume that the steady state has been reached for all 3 systems around 1.2 ns. After steady state system was reached, the heat flux per unit time across the cross-section was calculated from the slope of each curve was evaluated using least square fitting method and is listed in Table 4.

Along the same lines, the resultant temperature gradient due to steady state heat flux is plotted in Figure 21. As mentioned before, the system was divided into 100 slabs or layers. The temperature of each layer was calculated using 1000 samples stored at every 0.1 ps for 100 ps. The temperature was further block averaged over 13 such block-average temperatures. From the figure, it is quite clear that the temperature change across the slab in the un-thermostated zone is linear for all 3 systems. The slope, also known as temperature gradient was calculated by fitting the central portion of un-thermostated zone to avoid any boundary effects using least square method. The values of the temperature gradient for all 3 studied systems are also listed in Table 4.

Thereafter, the thermal conductivity for all three systems are listed in Table 2. The thermal conductivities of DETDA, EPON-862 and their crosslinked network were found to be 0.20, 0.21 and 0.30 W/m-K, respectively. Although, the experimental values of thermal conductivities of DETDA and un-crosslinked EPON-862 were not found it literature, the thermal conductivity of crosslinked epoxy network has been mentioned between 0.2 and 0.3 W/m-K.[27] Considering the fact, the calculated thermal conductivity is indeed in good agreement with experimental findings. Hence, non-equilibrium molecular dynamics simulation presents a positive route towards studying and predicted thermal properties of disordered or amorphous systems.

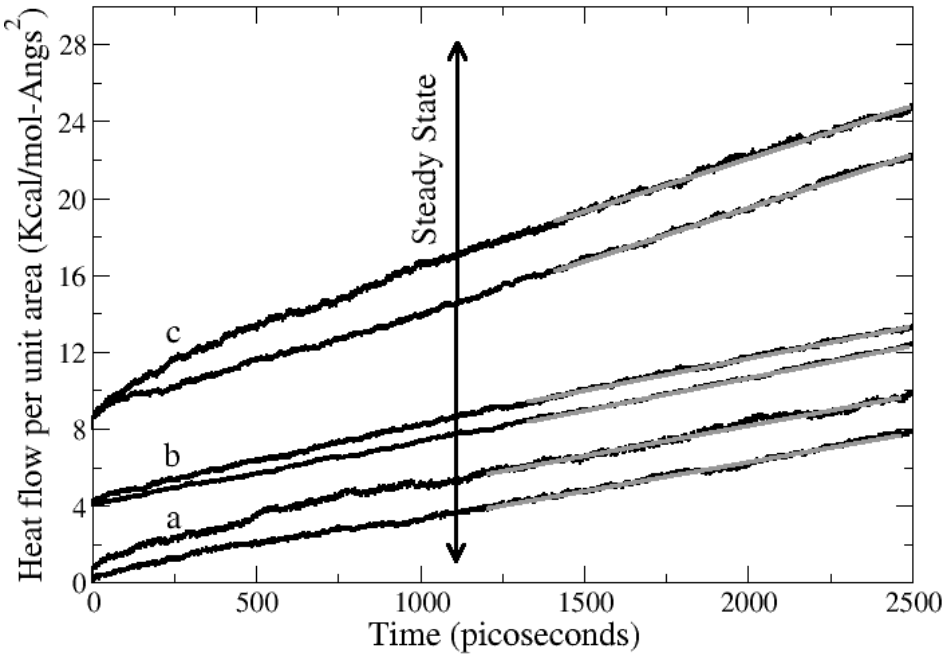

Figure 20: Heat Flux as a function of time. a) DETDA; b) EPON-862; c) crosslinked network. The plots for b) and c) are shifted by 4 and 8 kcal/mol-Å^2, respectively, for the sake of clarity. For each system, the above dataset represents the heat put in at high temperature region while lower dataset represent the heat taken off from low temperature region.

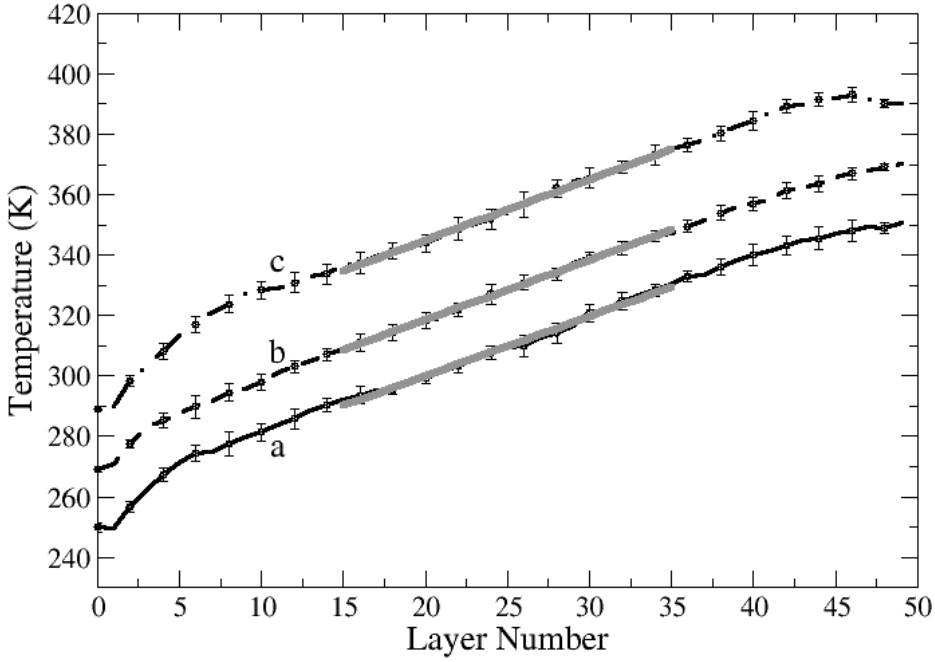

Figure 21: Temperature profile across slab for various studied systems. a) DETDA; b) EPON-862; c) crosslinked network. The plots for a) and c) are shifted by -15 K and 15 K respectively for the sake of clarity.

Thermal Conductivity of Crosslinked Network from Equilibrium Approach

Figure 22 shows the normalized heat flux autocorrelation function (as discussed previously) as a function of time for the crosslinked network along with uncrosslinked epoxy resin and curing agent. The figure also shows the thermal conductivity for all three systems as evaluated by integrating the heat flux autocorrelation function. It is observed from the figure that the autocorrelation function is oscillating and decays down to zero around ~2-3 picoseconds for EPON-862 and crosslinked system while it takes about 6 pico-seconds for DETDA. The difference in the decay times could be qualitatively attributed to the rigid and planar nature of the DETDA molecule unlike EPON and the network which contain flexible ether connecting linkages.

The figure also shows the trend of thermal conductivity vs. time as evaluated from the time integration of heat flux autocorrelation function. For all three cases, we find that the thermal conductivity first increases, then decreases and then becomes constant when the autocorrelation function decays down to zero. Such a trend in thermal conductivity has been previously observed for oscillatory decaying heat flux auto-correlation function[28]. From the plot, the thermal conductivities for DETDA, EPON-862 and their crosslinked system were found to be 0.15, 0.13 and 0.13 W/m-K at studied conditions.

Here, one can easily observe that the predicted thermal conductivity values using equilibrium MD are lower than their non-equilibrium counterpart. Here, one could attribute this to the system size effects. However, we would like to mention that we performed an equilibrium simulation for crosslinked network for system as big as twice of initial system with ~15000 atoms (please refer to Table 1). In that case too, we find the thermal conductivity values to be 0.13 W/m-K as with smaller crosslinked system. As we employed the same force-field for equilibrium and non-equilibrium simulations, the effect due to force field doesn't seem to play a significant role here. Hence, one could argue that non-equilibrium molecular dynamics simulations are possibly better suited for thermal conductivity prediction for crosslinked network systems.

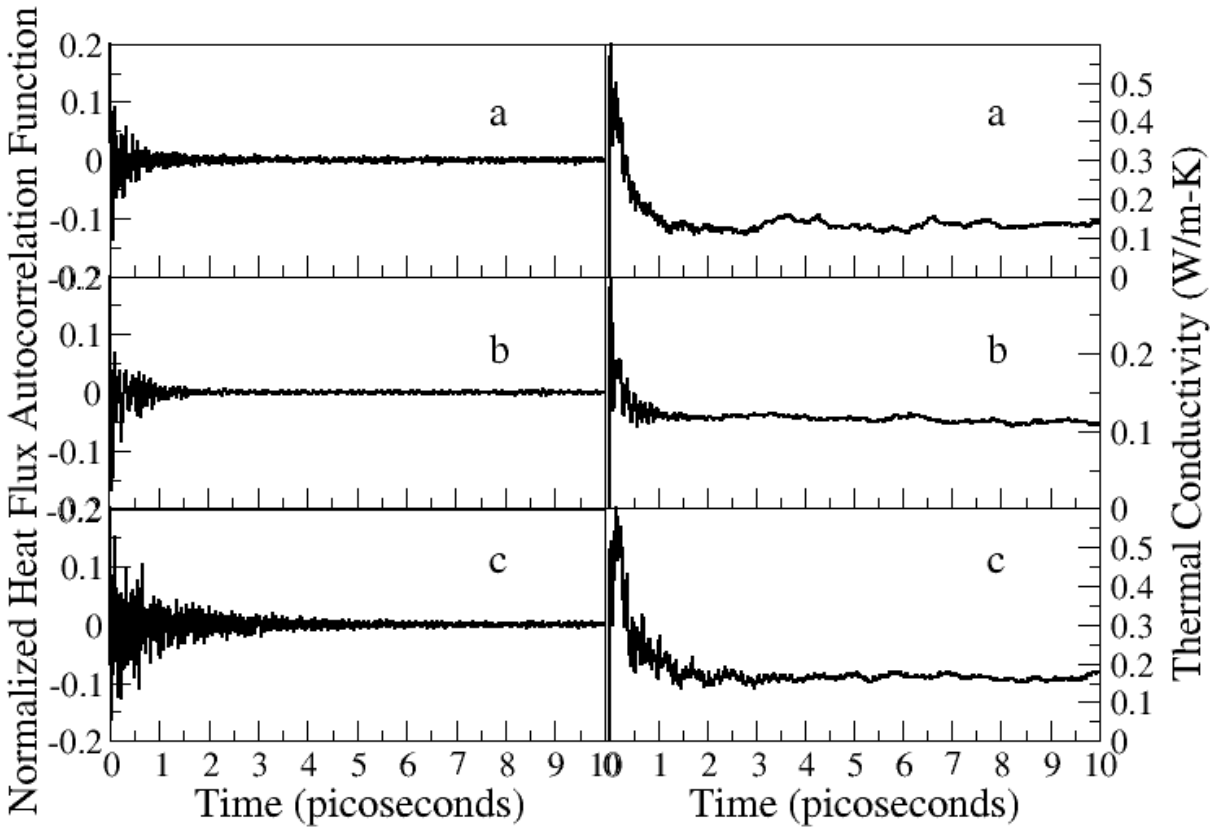

Figure 22: Normalized heat flux autocorrelation function and resultant thermal conductivities for various studied systems. a) crosslinked network ; b) EPON-862; c) crosslinked DETDA.

Table 4: Results from EMD and NEMD simulations of studied systems

System Studied	*Heat Flux (kcal/mol-Å2-ps)*	*Temperature Gradient (K/Å)*	*Thermal Conductivities (W/m-K)*	
			Non-Equilibrium Approach	*Equilibrium Approach*
DETDA	**3.08 x 10-3**	**0.53**	**0.20**	**0.15**
EPON-862	**3.08 x 10-3**	**0.55**	**0.21**	**0.13**
Crosslinked System	**5.12 x 10-3**	**0.60**	**0.30**	**0.13**

Power Spectrum Analysis

This section presents the analysis of different vibrations in the crosslinked network in terms of power spectrum of normalized velocity autocorrelation function (ACF) (Fourier Transform). The power spectrum presents the partial density of states for each atom and provides a perceptive regarding the energy storage in different parts of the molecule[28]. The partial density of states (PDOS) in terms of velocity autocorrelation function can be written as[29]

$$D_{p,\beta}(\omega) = c_\beta \int_0^\tau \Gamma_\beta(t)\cos(\omega t)\mathbf{d}t \quad \text{where} \quad \Gamma_\beta(t) = \sum_i^{N_\beta} \left\langle \mathbf{u}_{i\beta}(t) \bullet \mathbf{u}_{i\beta}(0) \right\rangle \Big/ \sum_i^{N_\beta} \left\langle \mathbf{u}_{i\beta}(0) \bullet \mathbf{u}_{i\beta}(0) \right\rangle$$

Here, $D_{p,\beta}(\omega)$ and $\Gamma(\omega)$ denote the PDOS and the normalized velocity autocorrelation function for atom type β. c_β denotes the concentration of species of type β. The total density of states is obtained by summing over the partial density of states.

$$D_\beta(\omega) = \sum_\beta D_{p,\beta}(\omega)$$

In this regard, Figure 23 shows the power spectrum of velocity ACF of various atomic entities in the crosslinked network. For these calculations, simulation was run for 40 picoseconds where data was stored at each timestep of 1fs. The power spectrum was evaluated from averaged velocity ACF over X, Y and Z directions as ACF was found to be isotropic in nature for atomic types. As one can see, the figure presents several peaks for each atomic type. These peaks represent different vibrations (stretching, bending, rocking, etc.) in which corresponding atomic entity is involved. In ordered systems, these are often termed as optical vibrations or phonons and are indeed captured using spectroscopic techniques such as IR, Raman spectroscopy, etc. These vibrations are known to be rarely involved in thermal transport through the system. The figure also presents a low broad low frequency peak which is present for all atomic entities. The peak is better depicted in figure 24. Generally, these peaks occur below low frequency limit of IR spectroscopy (~400 cm^{-1}) and are associated which acoustic modes of vibrations which are often responsible for thermal conduction across the system. For our system, we see one such broad peak, present in all power spectra of all atomic entities. The similar position of the peak in all atomic types suggests that indeed all entities are coherently involved in such low frequency vibrations. However, the broadness of the peak over several THz suggests a possible distribution of relaxation times with different overlapping low frequency vibrational modes. Recently, McGaughey et al. did a thermal conductivity analysis of metal organic framework (MOF-5) crystal[28]. The power spectrum analysis from their work give rise to several sharp peaks in the low frequency vibrational regime (acoustic region) unlike our work where we observe only one broad peak. Here, the differences in the peak characteristics in low frequency regime could be attributed to the disordered and amorphous nature of our system.

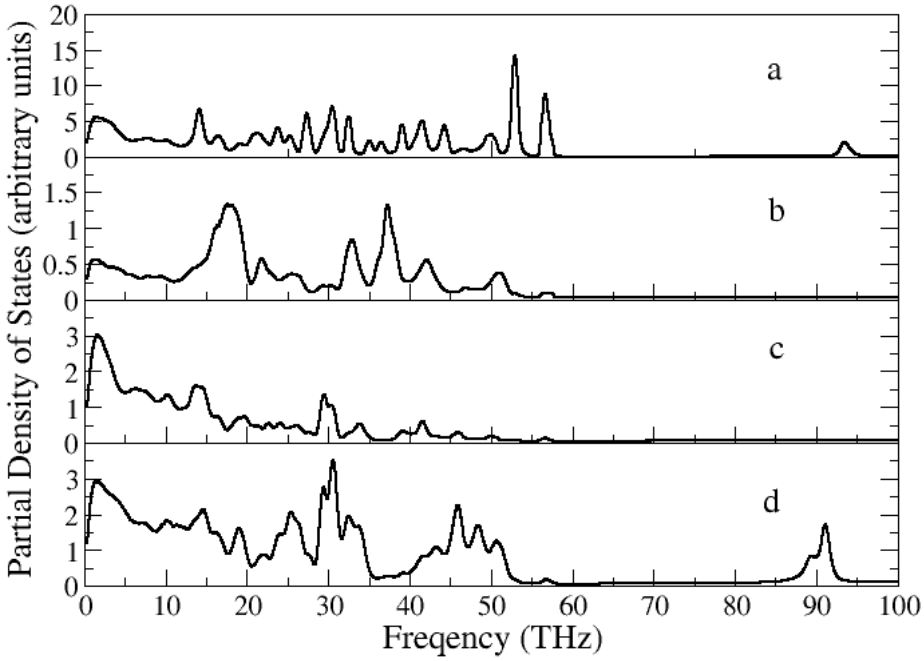

Figure 23. Power spectra of velocity autocorrelation function of various atomic entities of crosslinked network. a) sp^2 benzene carbon; b) amine nitrogen; c) ether and hydroxyl oxygen; and d) sp^3 carbon in methyl and methylene groups.

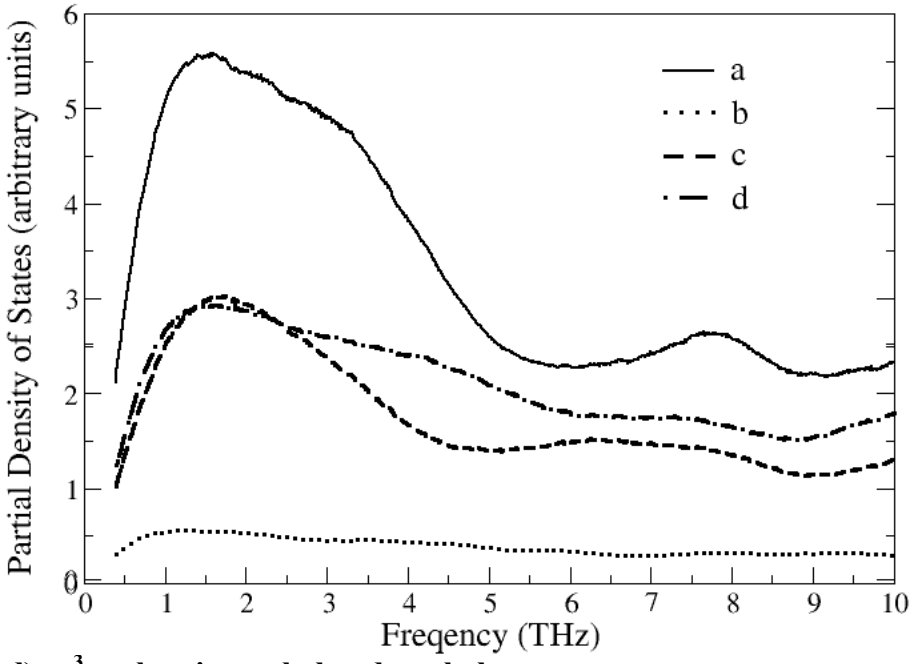

Figure 24. Low frequency power spectra of velocity autocorrelation function of various atomic entities of crosslinked network. a) sp^2 benzene carbon; b) amine nitrogen; c) ether and hydroxyl oxygen; and d) sp^3 carbon in methyl and methylene groups.

Pair Contribution Analysis

Although the results from equilibrium molecular dynamics simulations provide a lower estimate of thermal conductivity, it should be interesting to study the contribution of different interactions towards thermal conductivity. The heat flux equation shows that the heat flux indeed comprises of several terms. These terms are associated with a) kinetic energy; b) van der Waals potential energy; c) electrostatic potential energy; d) forces due to van der Waals interactions; e) forces due to electrostatic energy (within a certain cutoff, calculated in real space); and f) forces due to long range electrostatic interactions (outside the cutoff, calculated in Fourier space).

In order to capture different contributions, each term was evaluated separately and was stored for each timestep during the course of the simulation. As an example, in order to evaluate thermal conductivity due to kinetic and potential energy contributions only, we summed up the terms associated with a) and b) when calculating heat flux, while ignoring other terms. For our analysis, we represent the contribution or ignorance in terms of index "1" and "0", i.e., "1" represents the inclusion of the term while "0" suggests that a particular term is being ignored while calculating heat flux. For example, contribution description "100000" suggests that only kinetic energy contributions are taken into consideration while ignoring others during heat flux contribution. We believe that such an approach should take care of possible cross-terms as well in an implicit manner.

In this regard, several contributions are listed in Table 5 along with the resultant thermal conductivities and are graphically shown in Figure 25. On close observation, one could conclude that

a) The contributions from force terms have a dominating effect than energy terms towards final thermal conductivity. Please compare rows (1-4) vs. (5-12) in Table 5. Such a behavior has also been reported earlier for ionic systems[20].

b) The contribution from the forces due to van der Waals interactions is the most dominating towards thermal conductivity (4th contribution). Please compare (5-12) vs. the rest.

c) The contributions due to long range electrostatic force terms are negligible. Please compare (2,3), (5,6) and (9,10). This suggests that such contributions could be neglected while doing thermal analysis for organic, neutral amorphous systems with low partial charges.

d) The contributions from the energy terms (kinetic and van der Waals) are low but significant. Please see (1, 4). In addition, kinetic energy provides additional contributions while combining with other terms. Please compare (1+7) with 10. This possibly suggests a positive contribution of cross-terms in heat flux autocorrelation function which involve kinetic energy contributions.

Surprisingly, the contributions from electrostatic energy and short forces due to short range electrostatic interactions were observed to be negative. Please compare (2 and 4), (10 and 11)

and (10 and 12). Such a trend suggests that the cross-terms involving the electrostatic interactions and forces are contributing negatively towards the heat flux autocorrelation function.

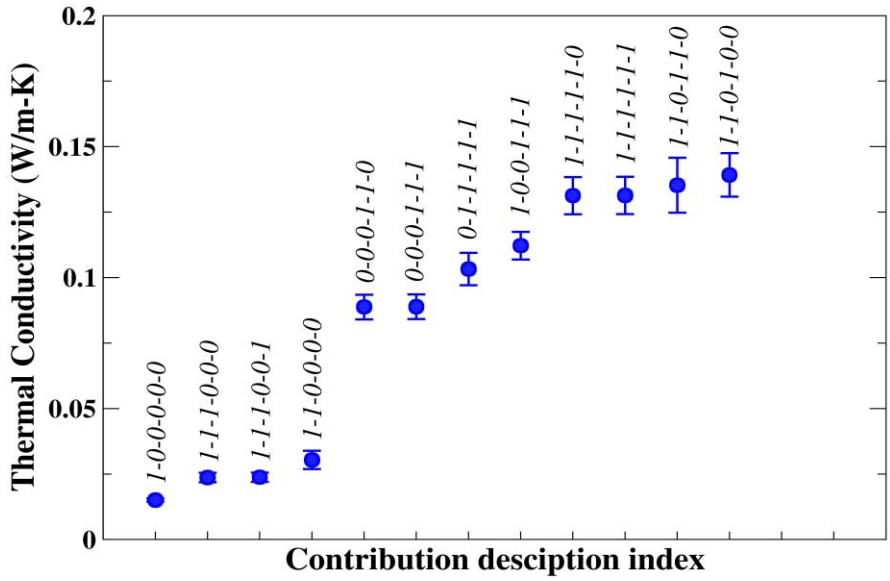

Figure 7. Thermal conductivity values for different heat flux component contributions. The details for each contribution index are listed in Table 3.

Table 5: Thermal Conductivities for different heat flux contributions.

	Contribution Description	λ (W/m-K)	Standard Deviation
1	100000	0.0151	0.0006
2	111000	0.0237	0.0018
3	111001	0.0238	0.0018
4	110000	0.0304	0.0035
5	000110	0.0888	0.0047
6	000111	0.0889	0.0047
7	011111	0.1033	0.0062
8	100111	0.1122	0.0053
9	111110	0.1313	0.0071
10	111111	0.1314	0.0071
11	110110	0.1353	0.0105
12	110100	0.1392	0.0083

Thermal Diffusivity and Mean Free Path Analysis

In addition to thermal conductivity, thermal diffusivity and heat capacity are two very important properties governing the thermal characteristics of a material and are related through following equation.

$$D = \frac{\lambda}{\rho C_P}$$

where, D, λ, ρ and C_P are thermal diffusivity, thermal conductivity, density and specific heat capacity at constant pressure. For the estimation of thermal diffusivity, the molecular dynamics simulations provide a route to calculate the heat capacity of a system from the fluctuations in its potential energy as shown below[30].

$$C_P = \frac{\langle U^2 \rangle - \langle U \rangle^2}{k_B T^2}$$

For our system, we estimated the heat capacity of our system to be 1.74 J/g-K at 300K. The heat capacity also showed weak temperature dependence. From previous estimation of thermal conductivity of 0.3 W/m-K from non-equilibrium molecular dynamics simulations along with system density of 1.12 gm/cm^3, the thermal diffusivity of epoxy networks was estimated to be 0.154 mm^2/s at 300K which is in excellent agreement with experimental value of 0.157 mm^2/s.27 The thermal diffusivity of a material provides a measure of how fast the heat transport is taking place in a diffusive manner.

In order to gain further understanding regarding behavior and dynamics of heat diffusion, we performed thermal relaxation simulations on an elongated slab with the length of ~34 nanometers. Firstly, the entire slab was annealed and equilibrated at very low temperature to remove any history of thermal fluctuations. Thereafter, the 20 Å region in the centre of the slab was heated to desired temperature T_O. Once the central region was equilibrated at T_O, the thermostat was switched off and constant energy simulations were performed to simulate the one dimensional heat flow as a function of time. The simulations were performed for desired temperatures, T_O of 100, 200, 300, 400, 500 and 600K. Two of such heat flow plots are shown in Figure 26 and 27 across the whole slab as a function of time for first 500 picoseconds. The figure shows that the temperature of the central region decays quite sharply while the temperature of rest of the slab builds up over time.

The temperature decay for the central slab is better depicted in Figure 28. In this figure, the decay has been normalized in order to differentiate the relative behavior of the central region. It is clear from the figure that higher initial temperature difference leads to sharper decay of central slab temperature. In order to understand the decay further, the plot was then fitted to stretched exponential curve with characteristic relaxation time, τ. The corresponding stretching factor β and relaxation time τ are shown in Table 6. The non-unity values of β suggest that there exists a distribution of relaxation times which could be associated with the low frequency vibrational

modes necessary for heat diffusion. Although, β increases with temperature, its non-unity value suggests that heat transport is indeed a phenomenon associated with a distribution of vibrational modes, irrespective of temperature, and hence a distribution of relaxation times. The table also shows the τ decreases as the temperature difference increases. Such a decrease could suggest the shift of relaxation times towards lower values, associated with more vibrant motions at high temperatures. It is also interesting to see that the distribution behavior of relaxation times is much more sensitive at low temperatures ($< T_g$) than high temperature ($> T_g$).

Given the diffusivity of the system, it is possible to correlate this relaxation time τ with a length scale. This length scale should provide a measure of how far the thermal transport has been reached before the local equilibrium has occurred, as associated with τ. In order to observe that length scale and its temperature dependence for different studied T_O, we used one-dimensional analog of diffusivity equation shown below.

$$\left\langle l^2 \right\rangle^{1/2} = \sqrt{2D\tau}$$

To observe qualitative trends, thermal diffusivity was assumed to be independent of temperature. The results for all studied cases are presented in Table 7. The table shows that this length scale is of the order of few nanometers and decreases with increasing temperature difference. Such a decrease could be attributed to more number of vibrational modes, higher probability of vibrational scattering which lead to low values of relaxation time and hence low l.

The temperature dependence of this length scale suggests that this length scale should be associated with mean free length of vibrational modes in solids, i.e., epoxy networks in our case. In order to estimate the mean free length from experimental values, we used well known relation which relates diffusivity to the mean free length as shown below

$$D = \frac{1}{3} v l; \qquad v = \sqrt{E/\rho}$$

Here, E, ρ, v and D represent elastic modulus, density, sound velocity and thermal diffusivity of the material, respectively. For epoxy networks, using experimental values of E, ρ and D as ~2 GPa, 1.17gm/cm^3 and 0.157 mm^2/s, the mean free path l, was estimated to be ~8 nanometers at room temperature. It is interesting to observe that mean free length and observed length scale based on relaxation time and diffusivity calculations are at same order of magnitude. It should not come as a surprise that they indeed be closely associated. The former length scale is associated with the collision of low frequency vibrational modes, necessary for heat diffusion while the later provides a length scale of heat movement in order to drive local thermal equilibrium.

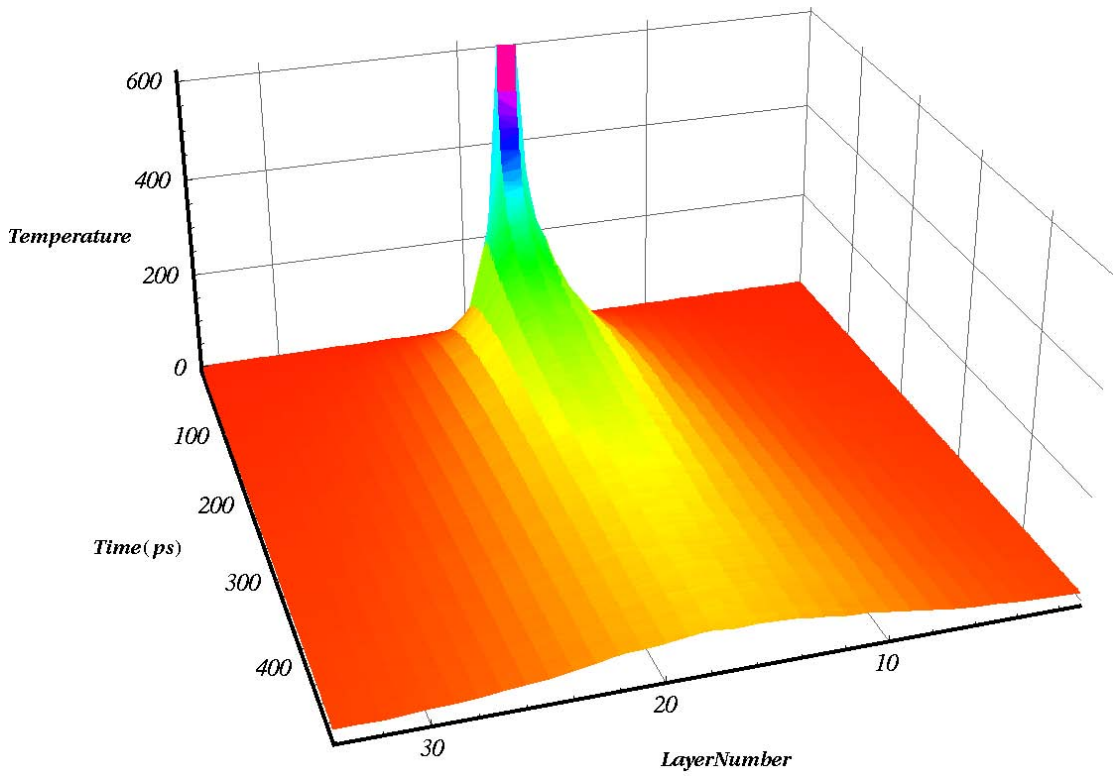

Figure 26. Temperature profile of the entire slab as a function of time. T_O = 600K.

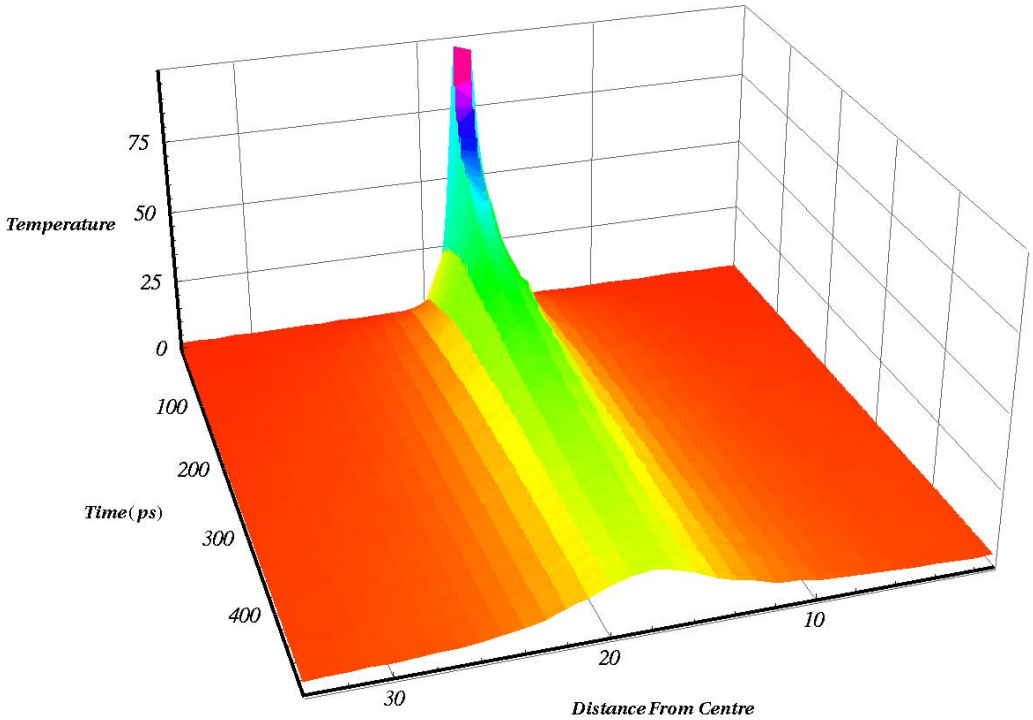

Figure 27. Temperature profile of the entire slab as a function of time. T_O = 100K.

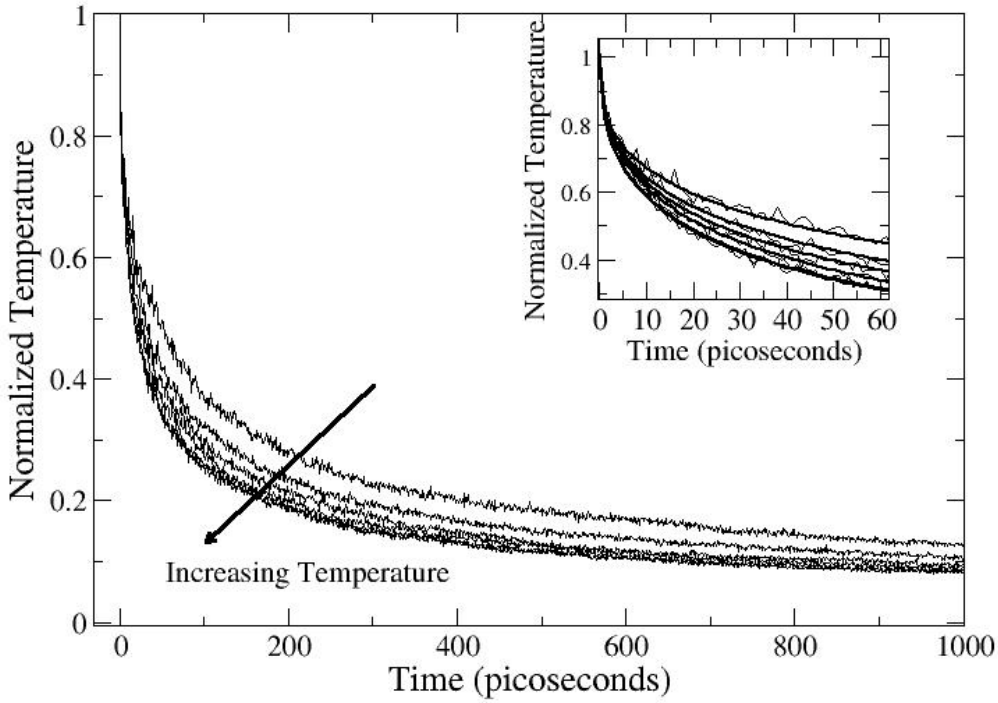

Figure 28. Normalized temperature decay profile of the central region for different starting T_O. Studied temperatures T_O were 100, 200, 300, 400, 500 and 600 K. The arrow points towards the direction of increasing temperature. Inset shows the stretched exponential fitting according to the parameters mentioned in Table 7.

Table 6: Stretched exponential fit[6] parameters and calculated length scale

Temperature T_O	Stretching Coefficient β	Characteristic Relaxation Time τ	$\langle l^2 \rangle^{1/2}$
100	0.39	107.7	57.5
200	0.41	73.9	47.7
300	0.43	59.7	42.8
400	0.45	50.2	39.3
500	0.44	43.6	36.6
600	0.45	38.0	34.1

[6] Fitted to the equation $T(t) = e^{-(t/\tau)^{\beta}}$

Thermal Conductivity Simulations for CNT/Epoxy Interface

The heat transport across CNT/epoxy network interface was also studied using molecular dynamics simulations. The CNT/epoxy network system which was build to perform such simulations is shown in Figure 29 and 30. For these simulations, the whole box was divided into 12 shells of 3 Angstroms each surrounding the CNT. In these simulations, the CNT at the centre of the slab was heated continuously while same amount of heat was taken about from the outermost shell. After a significant period of time (~200 ps), a thermal equilibrium was attained so that the temperature of the CNT and each of the shells was not changing with time. The temperature of CNT and each of the shells was then calculated from velocities and was block averaged using statistical methods. The temperature is plotted in Figure 31. It is very clear from the figure that indeed there exists a huge temperature gradient across the boundary of the CNT/epoxy interface. The temperature gradient is within one layer of epoxy with respect to CNT is about 10 times higher than temperature gradient across the whole box (~ 40 Angs), which suggest the dT/dx at the interface is about 2 order of magnitude higher with respect to epoxy materials. Such a simulation suggests a need of alternative approaches to create new pathways for the heat transport within epoxy composite materials.

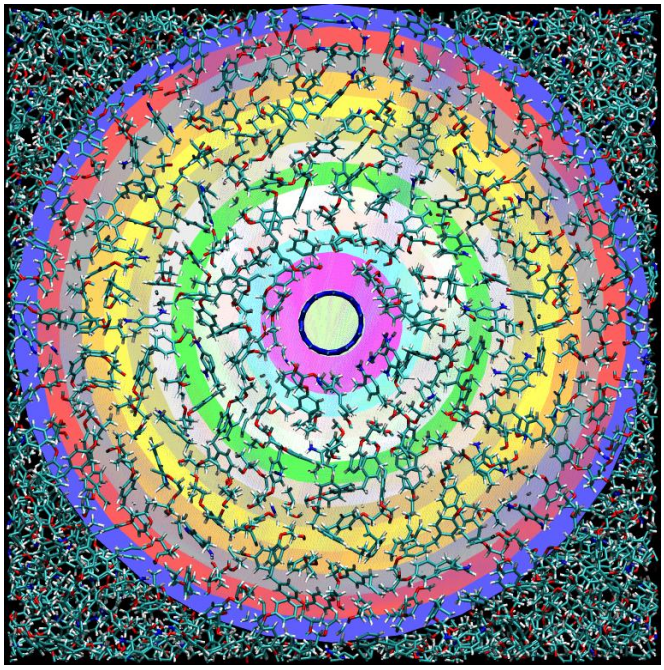

Figure 29: Top view of the CNT/Epoxy network system.

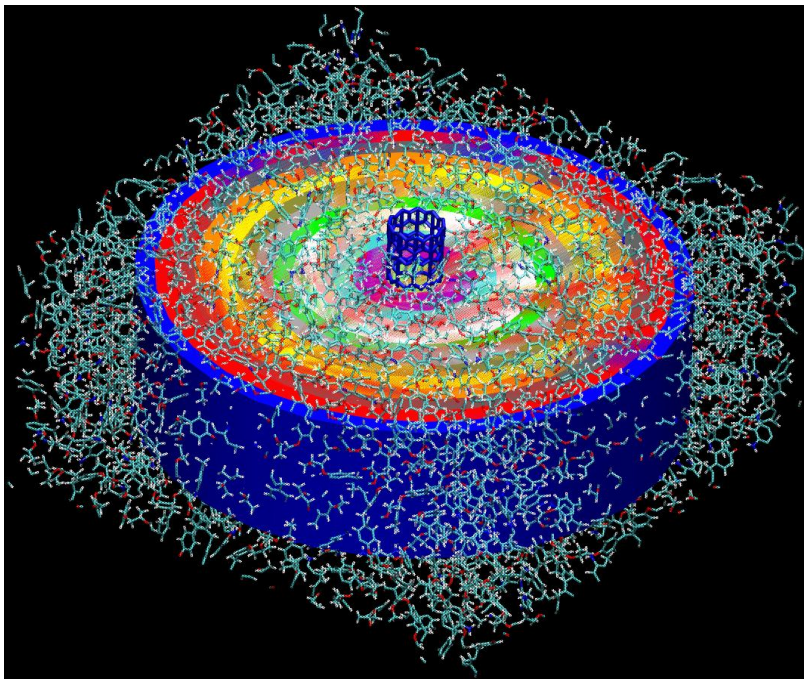

Figure 30: Slant view of the CNT/Epoxy system

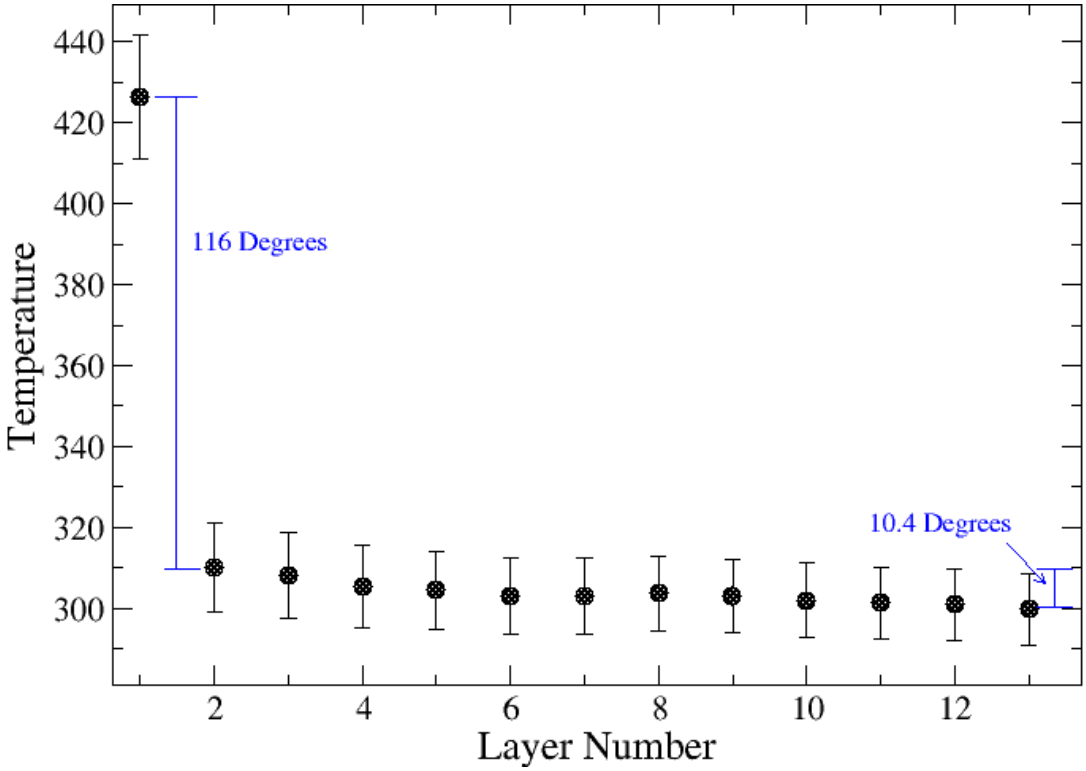

Figure 31: Temperature profile across CNT/epoxy interface and within epoxy matrix.

References

[1] Carslow, H. S.; Jaeger, J. C. Conduction of Heat in Solids, 2nd ed.; Oxford University Press: Oxford, 1986.

[2] Srivastava G. P. The Physics of Phonons, 2nd ed.; CRC Press: New York 1990.

[3] May, C. A., Ed. Epoxy Resins: Chemistry and Technology, 2nd ed.; CRC Press: New York, 1988.

[4] Sihn, S.; Ganguli, S.; Roy, A. K.; Qu, L.; Dai, L. Composites Science and Technology (accepted)

[5] Huang H.; Liu, C. H.; Wu Y.; Fan, S. Adv. Mater., 17 (13) 2005, 1652.

[6] P. L. Kapitza, J. Phys (USSR), 4, 181(1941).

[7] Frenkel, D.; Smit B. Understanding Molecular Simulation: From Algorithms to Applications; Elsevier: N.Y., 2002.

[8] Gou, J. H.; Minaie, B.; Wang, B.; Liang, Z. Y.; Zhang, C. Computational Materials Science 2004, 31, 225.; Fan, H. B.; Yuen, M. M. F Polymer 2007, 48, 1.;

[9] Heine, D. R.; Grest, G. S.; Lorenz, C. D.; Tsige, M.; Stevens, M. J. Macromolecules 2004, 37, 3857

[10]. N. Kondo, T. Yamamoto and K. Watanabe, e-J. Surf. Sci. Nanotech., 4, 239 (2006); M. A. Osman and D. Srivastava, Nanotechnology, 12, 21 (2004); Z. Yao, J. Wang, B. Li and G. Liu, Phys. Rev. B., 71, 085417 (2005); E. G. Noya, D. Srivastava, L. A. Chernozatonskii and M. Menon, Phys. Rev. B., 70, 115416 (2004); J. Che, T. Cagin and W. A. Goddard III, Nanotechnology, 11, 65 (2000); J. F. Moreland, J. B. Freund and G. Chen, Microscale Thermophysical Engineering, 8, 61 (2004); S. Berber, Y. Kyon and D. Tománek, Phys. Rev. Lett., 84 (20), 4163 (2000); K. Bi, Y. Chen, J. Yeng, Y. Wang and M. Chen, Phys. Lett. A, 350, 150 (2006); M. A. Osman and D. Srivastava, Phys. Rev. B., 72, 125413 (2005).

[11]. T. Kawamura, Y. Kangawa and K. Kakimoto, Phys. Stat. Sol. (c), 3 (6), 1695 (2006); Y. Yoon, R. Car, D. J. Srolovitz and S. Scandolo, Phys. Rev. B., 70, 012302 (2004).

[12]. S. R. Phillpot, P. K. Schelling and P. Keblinski, J. Mater. Sci., 40, 3143 (2005); W. Zenghui and L. Zhixin, Appl. Therm. Eng., 26, 2063 (2006); X. Feng, Z. Li, and Z. Guo, Microscale Thermophysical Engineering, 7, 153 (2003).

[13]. P. Chantrenne, M. Raynaud, D. Baillis and J. L. Barrat, Microscale Thermophysical Engineering, 7, 117 (2003).

[14]. R. Kubo, M. Toda, and N. Hashitsume, Statistical Physics II, Springer, Berlin, 1985.

[15]. D. J. Evans and G. P. Morris, Statistical Mechanics of Nonequilibrium Liquids, Academic Press, New York, 1990.

[16]. A. Maiti, G. D. Mahan, and S. T. Pantelides, Solid State Commun., 102 (7), 517, (1997).

[17]. S. Motoyama, Y. Ichikawa, Y. Hiwatari and A. Oe, Phys. Rev. B., 60, 292 (1999); B. Bernu and P. Vieillefosse, Phys, Rev. A, 18, 2345, (1978); B. R. A. Nijboer and F. W. De Wette, Physica (Utrecht), 23, 309 (1957).

[18]. N. Galama and C. A. Nieto de Castro, J. Chem. Phys., 120 (18), 8676 (2004).

[19]. C. V. D. R. Anderson and K. K. Tamma, Internat. J. Numer. Methods Heat & Fluid Flow, 14 (1), 12 (2004).

[20]. F. Bresme, B. Hafskjold and I. Wold, J. Phys. Chem., 100, 1879 (1996).

[21]. S. J. Plimpton, J. Comp. Phys., 117, 1 (1995) code available at http://lammps.sandia.gov.

[22]. Accelrys Inc, San Diego, CA, (module, Amorphous Builder).

[23]. P. Chantrenne and J-L. Barrat, Journal of Heat Transfer, 126, 577(2004).

[24] Wu, C. F.; Xu, W. J. Polymer 2006, 47, 6004

[25] Literature from resolution performance products,

http://www.resins.com/resins/am/pdf/SC1183.pdf

[26] Chiu, W.Y.; et al. Macromolecules 1994, 27, 3406

[27] Ganguli, S.; Roy, A. K.; Anderson, D. accepted in Carbon.

[28]. B. L. Huang, A. J. H. McGaughey, M. Kaviany, Internat. J. Heat and Mass Transfer. 50, 393 (2007).

[29]. C-K Loong, Phys. Rev. B, 45, 8052 (1992).

[30] Allen, M.P.; Tildesley, D. J. Computer Simulation of Liquids, Oxford University Press: Oxford, 1987